Nonlinear atomic force microscopy: Squeezing and skewness of micromechanical oscillators interacting with a surface

Karl-Peter Marzlin [1] Bryan Canam,[1] and Nisha Rani Agarwal [2]

[1]*Department of Physics, Saint Francis Xavier University, Antigonish, Nova Scotia, B2G 2W5, Canada*
[2]*Nano-Imaging and Spectroscopy Laboratory, Faculty of Science, University of Ontario Institute of Technology, 2000 Simcoe Street North, Oshawa, Ontario, ON L1G0C5, Canada*

We propose a two-frequency driving scheme in dynamic atomic force microscopy that maximizes the interaction time between tip and sample. Using a stochastic description of the cantilever dynamics, we predict large classical squeezing and a small amount of skewness of the tip's phase-space probability distribution. Strong position squeezing will require close contact between tip and surface, while momentum squeezing would also be possible in the van der Waals region of the tip-surface force. Employing a generalized Caldeira-Leggett model, we predict that surface-dependent dissipative forces may be the dominant source of quantum effects and propose a procedure to isolate quantum effects from thermal fluctuations.

I. INTRODUCTION

Surfaces and interfaces, i.e., the outermost layer of atoms of a material, define how it interacts with its surroundings [1]. It is therefore critically important to study the physical and chemical properties of surfaces. For more than three decades, atomic force microscopy (AFM) [2,3] has been an indispensable tool to explore the topography of surfaces and their electrical, magnetic, and elastic properties [4]. It has been applied to study a plethora of phenomena at the nanoscale, including the measurement of forces acting on individual molecules [5], the study of biological samples [6], and nanoparticles [7].

Conventional AFM consists of a cantilever with a nanometer-sized tip that interacts with the sample while being dragged over its surface (contact mode [2]). The properties of the sample, and in particular the force between tip and sample, are measured by monitoring the motion of the cantilever. In order to minimize the damage to the sample, the cantilever can be made to rapidly tap over the sample surface while scanning. The distance to the surface is manipulated by applying an oscillating, single-frequency piezoelectric force. This mode is known as dynamic AFM [8]. Our paper focuses on intermodulation AFM [9–11], where the cantilever is driven by a two-frequency force. Multifrequency AFM can increase the rate of data acquisition and enables us to monitor Fourier components of the tip's motion [12]. It can provide angstrom-scale resolution [13] and has been used to investigate the properties of magnetic surface forces [14] and dissipative forces [15,16].

Here, we describe the motion of the tip in dynamic AFM as a statistical system to accomplish several goals. First, a statistical description enables us to describe the dynamics of position and momentum variances, as well as that of higher-order correlations. Observing their dynamics could be used to study aspects of the tip-surface interaction that could not be measured by monitoring the tip's mean position alone. Measuring variance dynamics could become a new technique that increases the number of existing AFM imaging modes [12]. We focus on classical squeezing of thermal fluctuations, which could also be used to enhance the resolution of AFM. Squeezing in AFM has been studied before within a quantum-mechanical model by Passian and Siopsis [17,18]. Squeezing of thermal noise in a microcantilever with a parametric amplifier has been measured by Rugar and Grütter [19].

The generation of squeezing in AFM can be compared to classical nonlinear optics, where a coupling between different harmonics may trigger phase squeezing through the Kerr effect [20].

Squeezing of position and momentum variances only occurs under specific circumstances. Our second goal is therefore to provide a driving scheme that generates squeezing in dynamic AFM. We propose a scheme which maximizes the time the tip spends close to the sample in dynamic AFM. Such a scheme could also be useful to increase the signal in other AFM experiments.

Our third goal is to provide a statistical model that can clearly distinguish genuine quantum effects from classical dynamics. This is a nontrivial task because of the dissipative nature of the tip-surface interaction, which necessitates a description of the tip as an open quantum system [21]. In order to accomplish this, we have generalized the Caldeira-Leggett model [22] to a position-dependent dissipative force. A surprising result of this theory is that such a position-dependent dissipative force may be the dominant source of quantum effects in AFM. These findings may be relevant for other systems as well since there is a growing interest in quantum effects with micromechanical resonators [23–25] or even larger objects [26,27].

Our simulations indicate that under normal operations quantum effects in AFM are small compared to thermal

fluctuations. Our fourth goal is therefore to provide a method to separate quantum fluctuations from thermal noise. Noise cancellation methods have been successfully used in many areas in physics, including spin echoes [28], Doppler-free spectroscopy [29], force insensitivity in atomic [30,31] and molecular interferometry [32], and correlation measurements in AFM [33]. Generally, the development of further noise cancellation methods in AFM may lead to a significant increase in its sensitivity.

The paper is organized as follows. In Sec. II, we present the driving scheme to maximize the interaction time. Sections III and IV are devoted to the description of the cantilever as a statistical system. In Sec. V, we discuss our predictions for the generation of squeezing and skewness. We expound on the physics behind squeezing generation in AFM and the influence of quantum fluctuations in Sec. VI, which also contains a proposal for the elimination of thermal noise. This is followed by a conclusion in Sec. VII. Several appendices contain the details of our theoretical derivations.

II. DRIVING SCHEME TO MAXIMIZE SURFACE INTERACTION

Cantilever and tip in AFM form a complex mechanical system that may include bending motion and torsion [18], but a simple harmonic oscillator model often suffices and will be used here. The tip is described in phase space as a point particle with position $x(t)$ and momentum $p(t)$ and its dynamics is governed by Newton's second law:

$$\dot{p} = -kx - \gamma_Q p + F_{dr}(t) + F_{SF} + F_{dis}. \qquad (1)$$

Here, x denotes the position of the tip above the sample surface. The tip is in the engaged position with the sample for $x \approx -h$. Position $x = 0$ corresponds to the equilibrium position of the free tip, and k denotes the spring constant of the cantilever. Rate γ_Q describes internal mechanical losses of the cantilever. $F_{dr}(t)$ denotes a driving force that puts the cantilever in motion. The tip-surface interaction is decomposed into a conservative part F_{SF} and a dissipative part F_{dis}. The dissipative part arises from the deformation of the sample surface due to the interaction with the tip. It can be modeled in different ways, for instance through Kelvin-Voigt viscoelastic dissipation [34], a hysteretic force [35,36], a convolution integral [37], or a retarded response to the sample [38]. In this paper, we follow Ref. [39] and model the dissipate surface force by a position-dependent drag force, $F_{dis} = -\gamma(x)p$. In dynamic AFM, the driving force typically takes the form of a homogeneous force with one or two frequency components. Here, we consider two angular frequency components ω_1 and ω_2:

$$F_{dr}(t) = F_1 \sin(\omega_1 t + \phi_1) + F_2 \sin(\omega_2 t + \phi_2), \qquad (2)$$

with ϕ_1 and ϕ_2 controlling the relative phase of the force components. In absence of the sample, this model corresponds to an elementary driven damped harmonic oscillator. After a transient period, the oscillator will settle to a steady-state motion of the form

$$x_0(t) = \frac{F_1}{M\omega_1} \text{Im}\left(\frac{e^{i\omega_1 t + i\phi_1}}{Z(\omega_1)}\right) + \frac{F_2}{M\omega_2} \text{Im}\left(\frac{e^{i\omega_2 t + i\phi_2}}{Z(\omega_2)}\right), \qquad (3)$$
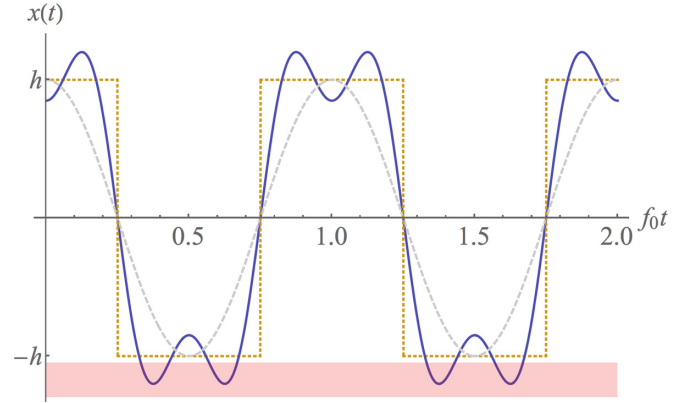

FIG. 1. Proposed driving scheme. For a periodic motion, the tip would remain close to the sample (red rectangle near $x = -h$) if the motion would take the form of a square wave (orange dotted curve). In single-frequency AFM (gray, dashed), the tip spends little time near the sample, but the suggested two-frequency driving scheme (blue, solid) approximates a square wave.

where

$$Z(\omega) = \frac{\omega_0^2 - \omega^2}{\omega} + i\gamma_Q \qquad (4)$$

is the mechanical impedance of the cantilever. M denotes the reduced mass of cantilever and tip, and $\omega_0 = 2\pi f_0 = \sqrt{k/M}$ denotes the resonance angular frequency.

The principle of the proposed driving scheme is explained in Fig. 1. In dynamic AFM, the driving force induces a periodic motion of the cantilever. If the force could be arbitrarily strong, the interaction time with the surface would be maximized for a square wave motion, where the tip spends half the time period close to the surface during each cycle. In a two-frequency driving scheme, one can maximize the time the tip spends near the surface if the two frequency components of the motion correspond to the first two Fourier coefficients of a square wave. Equation (3) implies that this can be achieved if we pick the driving frequencies as $\omega_2 = 3\omega_1$, and the force amplitudes so that they produce the Fourier coefficients, $\frac{F_1}{M\omega_1}\text{Im}\,e^{i\phi_1}Z^{-1}(\omega_1) = \frac{4}{\pi}h$ and $\frac{F_2}{M\omega_2}\text{Im}\,e^{i\phi_2}Z^{-1}(\omega_2) = -\frac{4}{3\pi}h$. For the choice $\omega_1 = \omega_0$, $Z(\omega_0)$ is imaginary and $Z(3\omega_0)$ is a negative real number for $\gamma_Q \ll \omega_0$. The phases then can be chosen as $\phi_1 = 0$ and $\phi_2 = \frac{\pi}{2}$.

The two-frequency driving scheme proposed above could be extended to generate higher-order Fourier components of a square wave. This would require a multifrequency driving force with components that oscillate at an integer multiple of the lowest force frequency. Such a scheme would provide a more precise control about the location of the tip when it is close to the surface: in the scheme of Fig. 1, there would be more oscillations with smaller amplitude around the lowest location of the tip. However, such a higher-order scheme would require control about the relative phases of all frequency components. We will see below that, even in the context of two frequencies, the optimal choice of phases is affected by the tip-surface interaction. We therefore anticipate that implementing higher-order schemes will require further analysis.

In many intermodulation AFM experiments, the two driving frequencies are only separated by a few hundred Hz [39]. This has the advantage that one can probe the Fourier transform of the cantilever motion at multiples of the frequency difference, i.e., at high resolution in frequency space. However, to generate strong coupling between different probability moments (see Sec. III), the larger frequency should be a harmonic of the lower frequency.

III. DYNAMICAL EQUATIONS FOR PROBABILITY MOMENTS

A real tip is not a point particle, and its motion is generally subject to thermal or quantum fluctuations, which require a probabilistic description. The position of the tip is then replaced by the mean position $\bar{x}(t) = \langle x \rangle$. Here, angle brackets denote averaging with respect to a probability distribution, which can be of classical or quantum nature. Variances are described through mean values of quadratic expressions, such as $\Delta x^2 = \langle (x - \bar{x})^2 \rangle$. More generally, one can characterize a probability distribution through its moments [40]:

$$\Delta_{n,m} = \tfrac{1}{2} \langle (x - \bar{x})^n (p - \bar{p})^m + (p - \bar{p})^m (x - \bar{x})^n \rangle. \quad (5)$$

In a classical description, the ordering of position and momentum terms is irrelevant, but we keep a symmetric ordering so that our formalism can be used for a quantum description as well. Second-order moments describe position variance $\Delta x^2 = \Delta_{2,0}$, momentum variance $\Delta p^2 = \Delta_{0,2}$, and cross-correlation $\Delta_{1,1}$. Higher-order moments describe a non-Gaussian structure of the distribution. For instance, $\Delta_{3,0}$ describes the skewness in position, which is a measure for how much the maximum of the distribution differs from mean value $\bar{x}$ (see Sec. IV).

The driving scheme introduced above has the potential to induce a large amount of squeezing and a small amount of skewness in the probability distribution. Squeezing refers to the reduction of the variance of one observable, say Δx, at the expense of increasing the variance of its conjugate variable Δp. It is most often considered in the quantum description of light, and it is sometimes assumed that the coupling of stretching Δp while squeezing Δx is a consequence of Heisenberg's uncertainty principle. However, squeezing also occurs in classical probability distributions, where the coupling of stretching and squeezing is a consequence of the conservation of phase-space volume for conservative forces because of Liouville's theorem [41].

For a point particle, the dynamical equations take the form $\dot{p} = F(x)$, but for an object that is described through a probability distribution we have $\dot{\bar{p}} = \langle F(x) \rangle \neq F(\bar{x})$. This implies that the dynamics of mean position and momentum is generally coupled to higher-order moments. For instance, $F(x) = cx^3$ would couple mean momentum $\bar{p}$ to skewness $\Delta_{3,0}$.

For a force that is not given by a power law, the dynamical equation $\dot{\bar{p}} = \langle F(x) \rangle$, and the equivalent equations for all moments, will not generate a closed set of equations for mean values, variances, and skewness (see Appendices A and B). To overcome this problem, we make a *localization approximation*: we assume that the probability distribution of the oscillator is so narrow that the force varies little over the width of the distribution. In this case, the mean force can be expanded as a Taylor series around the mean position:

$$\langle F(x) \rangle \approx \sum_{n=1}^{n_{\max}} \frac{F^{(n)}(\bar{x})}{n!} \langle (x - \bar{x})^n \rangle = \sum_{n=1}^{n_{\max}} \frac{F^{(n)}(\bar{x})}{n!} \Delta_{n,0}. \quad (6)$$

We have used the localization approximation to derive a coupled set of equations for mean position $\bar{x}$ and momentum $\bar{p}$, as well as all moments $\Delta_{n,m}$ up to third order, $(n, m) \in \{(2, 0), (1, 1), (0, 2), (3, 0), (2, 1), (1, 2), (0, 3)\}$. The result is rather lengthy and given by Eqs. (B26)–(B34). As an example, the dynamical equation for mean momentum takes the form

$$\dot{p} = F - (\gamma_Q + \gamma)\bar{p} + \frac{\Delta_{2,0}}{2}(F'' - \bar{p}\gamma'') - \gamma' \Delta_{1,1}$$
$$+ \frac{1}{6}\Delta_{3,0}(F^{(3)} - \bar{p}\gamma^{(3)}) - \frac{1}{2}\gamma'' \Delta_{2,1}. \quad (7)$$

In this expression, functions F and γ depend on the mean position, e.g., $F = F(\bar{x})$. We have derived these equations from a classical stochastic theory (Fokker-Planck equation, see Appendix A) and from a Lindblad-type master equation for open quantum systems (Appendix B). The results differ by genuine quantum terms, which are proportional to $\hbar^2$ in Eqs. (B26)–(B34). In addition, there is a technical difference between both derivations that only concerns the position-dependent dissipative surface force. This difference is discussed in Appendix B.

IV. TIP FLUCTUATIONS: SQUEEZING AND SKEWNESS

Suppose we know the moments $\Delta_{n,m}$, either by measuring it or by solving the dynamical equations. Can we find the probability distribution that describes the stochastic state of the oscillator? The answer is yes, and follows from the reconstruction theorem in quantum physics [42], for instance. In Appendix C, we derive an approximate expression for a classical phase-space probability distribution $\rho(\boldsymbol{r})$ in terms of moments, where bold symbols $\boldsymbol{r} = (x, p)$ denote phase-space vectors. A multivariate skew-normal probability distribution $\rho(\boldsymbol{r})$ can be expressed as the product of a Gaussian distribution $\rho_0(\boldsymbol{r})$ and a second function Φ [43]:

$$\rho(\boldsymbol{r}) = \rho_0(\boldsymbol{r})\Phi(\boldsymbol{r}), \quad (8)$$

$$\rho_0(\boldsymbol{r}) = \frac{1}{2\pi |C|^{\frac{1}{2}}} e^{-\frac{1}{2}(\boldsymbol{r} - \bar{\boldsymbol{r}})^T \cdot C^{-1} \cdot (\boldsymbol{r} - \bar{\boldsymbol{r}})}, \quad (9)$$

$$C = \begin{pmatrix} \Delta_{2,0} & \Delta_{1,1} \\ \Delta_{1,1} & \Delta_{0,2} \end{pmatrix}. \quad (10)$$

The eigenvalues of correlation matrix C are denoted by σ_1^2 and σ_2^2, where σ_1 corresponds to the larger and σ_2 to the smaller phase-space variance. If the eigenvectors of C are aligned with position and momentum, position squeezing corresponds to $\Delta x = \sigma_2$ and $\Delta p = \sigma_1 > \sigma_2$ [55]. The Gaussian factor $\rho_0(\boldsymbol{r})$ would then have an ellipsoid form that is stretched along the p axis and squeezed along the x axis. In general, however, squeezing can occur along any direction in phase space.

If only information about second-order moments is available, the Gaussian part is all that can be known about ρ.

Knowledge about third-order moments enables us to find the following expansion of $\Phi(r)$ around the mean position $\bar{r} = (\bar{x}, \bar{p})$:

$$\Phi(r) = 1 + S \cdot R + \frac{1}{6} \sum_{i,j,k} \mu_{ijk} R_i R_j R_k + O(R^4), \quad (11)$$

$$S_i = -\frac{1}{2} \sum_{j,k} \mu_{ijk}(C^{-1})_{jk}, \quad (12)$$

$$R = C^{-1} \cdot (r - \bar{r}), \quad (13)$$

where $\mu_{111} = \Delta_{30}$, $\mu_{222} = \Delta_{03}$, and $\mu_{112} = \mu_{121} = \mu_{211} = \Delta_{21}$, as well as $\mu_{221} = \mu_{212} = \mu_{122} = \Delta_{12}$. Vector S corresponds to the shift of the maximum of ρ relative to the mean position $\bar{r}$, as long as $|S|$ is much smaller than the variances of ρ. The third-order term (the triple sum) generates a roughly triangular distortion of the Gaussian profile.

In the following, we will solve the dynamical equations of motion and use the reconstructed classical probability distribution to visualize the effect of the surface force on variances.

V. RESULTS

To analyze the evolution of the probability distribution $\rho(r)$, we have solved the dynamical equations (B26)–(B34) in two different ways. A numerical solution was found using the software package MATHEMATICA, with details given in Appendix D. In addition, we evaluated the effect of the surface forces using first-order perturbation theory, with details provided in Appendix E.

The results of both methods indicate that a classical description is perfectly adequate for typical AFM oscillators. In the discussion below, we will describe under which circumstances quantum effects may become relevant, and how one can isolate surface-induced quantum effects from classical surface-induced effects. Furthermore, both methods predict that the evolution of mean position and momentum is only very weakly affected by the coupling to probability moments. For this reason, we will concentrate on discussing squeezing and skewness.

In our numerical simulations, we have considered a cantilever with a resonance frequency of 300 kHz, and a quality factor of $Q = 400$, and studied the time evolution for up to 200 cycles. This is a typical duration for many AFM experiments, and it is sufficiently long to induce strong squeezing. We have considered several different cases, including single-frequency on- and off-resonant driving, as well as two-frequency driving with different sets of frequencies ω_i and phase factors ϕ_i in driving force (2). Figures 2 and 3 show the reconstructed probability distribution at the time when the tip is close to the sample during cycle 102 and 198, respectively [56]. For this specific case, we have used $\omega_1 = \omega_0$, $\omega_2 = 3\omega_0$, as well as $F_1 = 1.21$ nN and $F_2 = 950$ nN. The second force component needs to be much stronger to compensate for the fact that it drives the cantilever off-resonantly. The phases of the force were chosen as $\phi_1 = \pi$ rad and $\phi_2 = 2.67$ rad. This choice of phases is rather different from the phases presented at the end of Sec. II for reasons we will discuss below.

We have chosen to display the reconstructed probability distribution after 102 cycles, because at this time triangular
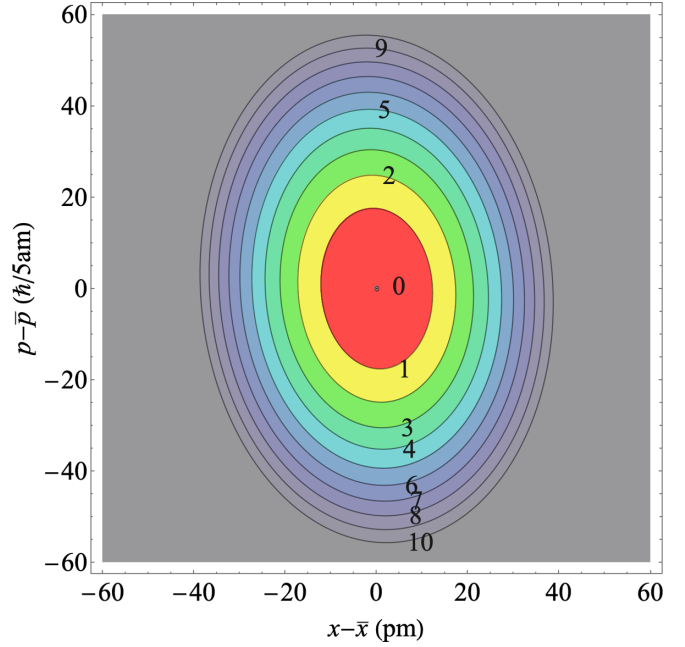

FIG. 2. Contour plot of the reconstructed classical probability distribution after 102 cycles. A contour labeled with n corresponds to a reduction of the probability density by an amount e^{-n} compared to the maximum value.

distortions of the Gaussian distribution, i.e., the triple sum in Eq. (11), are strongest. Since these distortions grow with the third power of the distance vector R_i from the mean position of the tip, their effect is more pronounced far away from the center of the distribution. However, even on the outermost contour in Fig. 2, the deviation from a Gaussian shape only amounts to about 2% and is barely visible. Shift vector S of Eq. (12), which quantifies skewness, is negligibly small at this time, about 0.01 pm.

After 198 cycles, strong squeezing can be observed [see Fig. 3(a)]. For our choice of parameters, we observe almost a pure position squeezing (i.e, the ellipse is almost vertical). Skewness has grown by a factor of 10 to about 0.15 pm. However, like triangular distortions, the effect is too small to be visible in our plots. The amount of squeezing is quantified through the ratio $\mathcal{R}$ of the large and small diameter of the probability distribution. The squeezing parameter is then defined as $r = \frac{1}{2} \ln \mathcal{R}$. We find a maximum value of $r = 1.01$ in the presence of a dissipative surface force [Fig. 3(a)] and $r = 1.24$ in absence of a dissipative surface force [Fig. 3(c)]. By comparison, Passian and Siopsis [18] predict a smaller squeezing parameter of 0.23. The difference is explained by the fact that Ref. [18] considers the attractive van der Waals regime of the surface force. In this regime, our simulations for a weakly driven tip that is never in contact with the sample surface predict a similar amount of squeezing. In their experiment with a parametric microamplifier [19], Rugar and Grütter reported squeezing of thermal noise by 4.9 dB. By comparison, the squeezing parameter of $r = 1.24$ that we obtained in our simulation corresponds to a noise reduction of 8.8 dB. Preliminary data on squeezing in dynamic AFM have been reported by Ahlin [44] through observation of
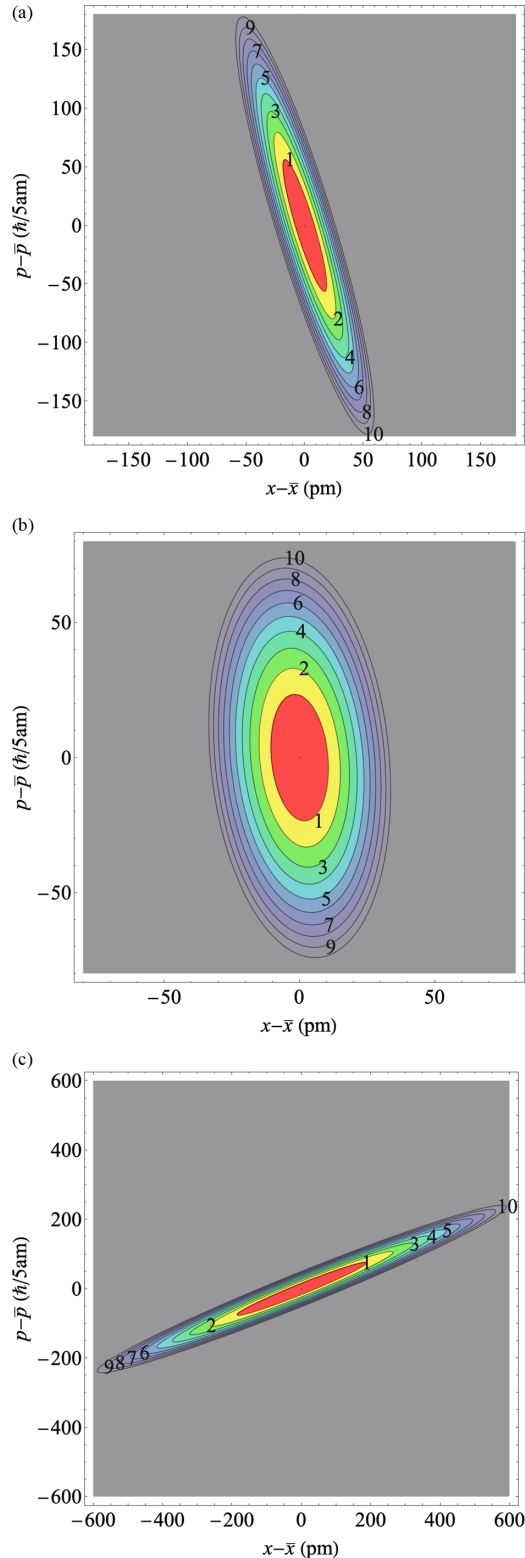
(a)

(b)

(c)

FIG. 3. (a) Contour plot of the reconstructed classical probability distribution after 198 cycles, for $\phi_1 = \pi$ rad and $\phi_2 = 2.67$ rad. (b) The same for $\phi_1 = 0$ rad and $\phi_2 = \frac{\pi}{2}$. (c) The same as panel (a) but with strongly reduced dissipative surface force.

noise spectra. Figure 5.5 of Ref. [44] suggests an amount of squeezing of about 7 dB, which is similar to the results of our simulations.
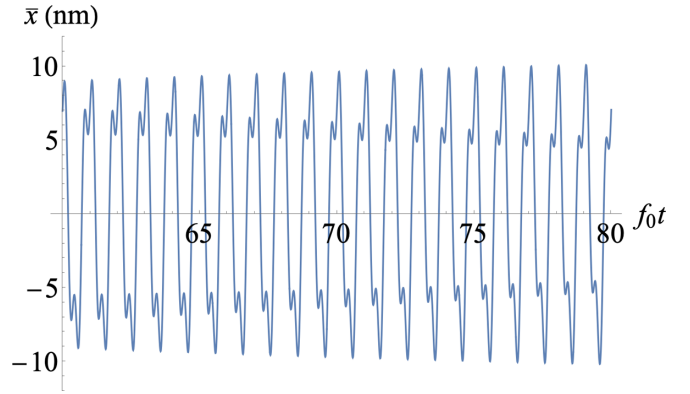

FIG. 4. Evolution of the tip's mean position over several periods $T = 1/f_0$ for a driving force with phase factors $\phi_1 = \pi$ rad and $\phi_2 = 2.67$ rad.

In our simulations, the amount of squeezing critically depends on the choice of phase factors for the driving force. For instance, Fig. 3(b) shows the same situation, but with phase factors chosen as described in Sec. II, which leads to a squeezing of $r = 0.43$. The reason for the strong reduction in squeezing is that the surface force has a strong influence on the double-peak structure in Fig. 1, which is key to increasing the tip-surface interaction time. In the presence of the surface, the double peak tends to become asymmetric, so that the tip is not in close contact with the surface for a longer time anymore (see Fig. 4). The reason for this strong influence is that the relative sign of the two Fourier components of the approximate square wave in Fig. 1 matters a lot for its overall shape. In the figure, the two Fourier components have opposite signs and thus cancel each other out close to the central peak. However, if they have the same sign, they add up to a more pronounced single peak.

In Fig. 4, one can see that the double-peak structure varies over time. The reason is that the frequencies of the two frequency eigenmodes are affected by the surface force [45]. The double peak therefore varies between an approximate square wave and a single peak. By adjusting the phase factors of the two driving force components, one can mitigate this effect to some extent and thus optimize squeezing. Another possibility would be to adjust the driving frequencies slightly, to compensate for the temporal variation of the double peak.

Finally, we have studied the effect of the dissipative surface force on squeezing by comparing the result of our full simulation Fig. 3(a) to a simulation in which the dissipate surface force is reduced by a factor of 10^{-3}. The result is shown in Fig. 3(c) and indicates that F_{dis} both suppresses squeezing and has a strong influence on the axis of the ellipse. We generally found that, without F_{dis}, one almost always obtains momentum squeezing rather than position squeezing when the tip is close to the sample.

VI. DISCUSSION

Our results show several general trends, which are discussed in this section.

The role of the *dissipative surface force* is twofold: it reduces the amount of squeezing, and it rotates the squeezing
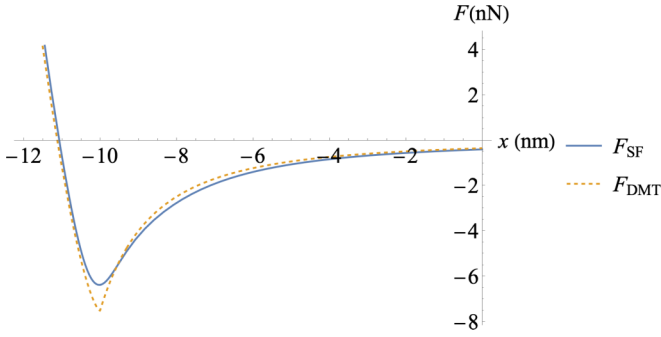
FIG. 5. Conservative surface force F_{SF} as a function of cantilever position x. The solid curve shows the modified Derjaguin-Muller-Toropov model (D2) used in this paper. The dashed curve displays the original DMT model (D1).

axis so that one can have (mostly) position squeezing instead of momentum squeezing. Since the fluctuation-dissipation theorem [46,47] predicts an increase of fluctuations if a dissipative force acts on a system, it is natural that squeezing is reduced; reducing variances simply becomes more difficult. In our dynamical equations, fluctuations are described by terms proportional to p_{th} in Eq. (B30). A dissipative force can change the orientation of the squeezing axis through its momentum dependence, which enables it to counteract features of the conservative surface force that will be discussed in the next paragraph.

The *conservative surface force* alone tends to create momentum squeezing. We conjecture that the reason for this is that, for most of the time during one oscillation cycle, the tip is moving in the long-range van der Waals tail of the surface force. As can be seen in Fig. 5, this tail has negative curvature, i.e., the force would pull particles that are closer to the sample stronger towards the surface than particles that are further away. Consequently, a phase-space probability distribution would then tend to be stretched along the spatial axis. Since F_{SF} is a conservative force, Liouville's theorem then implies squeezing in momentum direction.

Conversely, a conservative force with positive curvature would tend to squeeze the spatial direction of a probability distribution and stretch it in the momentum direction. For the Derjaguin-Muller-Toropov (DMT) force shown in Fig. 5, this is the case when the tip is in close contact with the surface ($x < -10$ nm). Furthermore, our numerical results suggest that this may also be the most effective way to achieve large squeezing. The reason is that the coupling between $\Delta_{1,1}$ and $\Delta_{0,2}$ [the first term on the right-hand side of Eq. (B30)], which is responsible for the generation of squeezing, is proportional to the gradient of the force. The gradient of the surface force is much larger in the contact region than in the van der Waals region, so that a larger amount of squeezing can be achieved. We emphasize, however, that this result does not support the idea that strong squeezing is simply a consequence of pressing the tip against a surface, which would produce position squeezing. This intuitive picture does not explain the orientation of the squeezing axis, which is sensitive to the entire dynamics during a cycle, as shown in Fig. 6. Position squeezing is the result of an interplay between a conservative and a nonconservative force, such as F_{dis}. The details of such
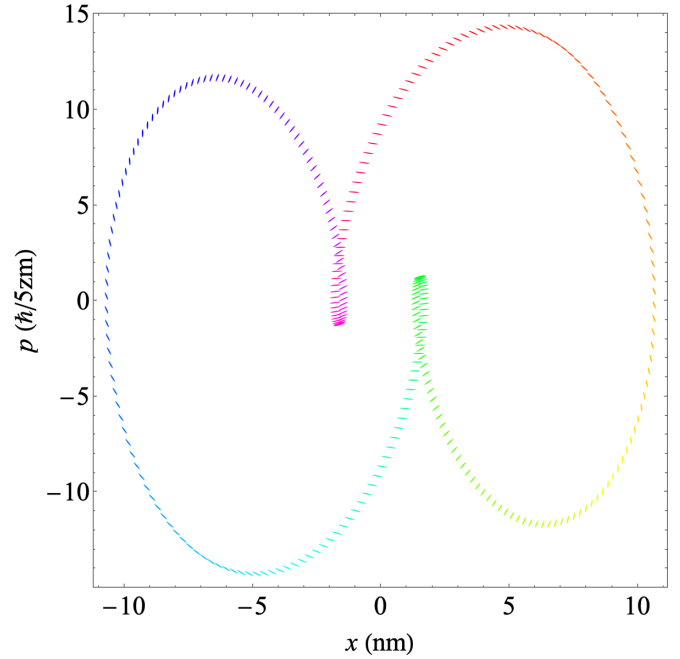

FIG. 6. Time evolution of the reconstructed probability distribution during the full 198th cycle. Each ellipse corresponds to the probability distribution at one particular time during the cycle, and is centered around the mean position of the tip at that time. The size of the ellipse corresponds to the mean variances of the distribution in phase space. For instance, the innermost ellipse in Fig. 3(a) corresponds to the leftmost ellipse in this figure. For better visibility, the size of each ellipse has been increased by a factor of 5.

an interplay are involved due to the overall dynamics of the tip during a cycle. For a two-frequency driving force, the tip's mean position follows a noncircular path. In addition, the axes of the ellipse oscillate at twice the resonance frequency. The latter effect is known from optical squeezing and follows from our perturbative treatment in Appendix E.

Quantum effects are generally negligible in our numerical simulations. To understand how they could be increased, we used first-order perturbation theory to study the influence of a dissipative surface force F_{dis} of form (B12). We concentrate on the dissipative part because it generates terms proportional to $\hbar^2$ in the dynamical equations for variances $\Delta_{2,0}$, $\Delta_{1,1}$, and $\Delta_{0,2}$, whereas the conservative surface force only introduces quantum terms for third-order moments. The first-order correction to the position variance is given by

$$\Delta_{20}^{(1)} = \gamma_0 \int_0^t dt' e^{-\gamma_Q(t-t')} e^{-\frac{\hbar}{x_\gamma}[1+\cos(\omega_0 t'+\phi_1)]}$$

$$\times \left[\frac{(L^4 - 16\Delta x_{th}^4)}{8\omega_0 x_\gamma^2} - \frac{\gamma_Q}{\omega_0} \frac{L^4}{8\Delta x_{th}^2} \sin[2\omega_0(t-t')] \right.$$

$$\left. - \frac{[L^4(\Delta x_{th}^2 + x_\gamma^2) - 16\Delta x_{th}^6]}{8\Delta x_{th}^2 x_\gamma^2} \cos[2\omega_0(t-t')] \right].$$

$$(14)$$

This result applies to the case of a single-frequency driving force [$F_2 = 0$ in Eq. (2)]. In this case, the unperturbed mean position (3) varies like $x_0(t) = h\cos(\omega_0 t + \phi_1)$.

In Eq. (14), all quantum terms are proportional to L^4. Compared to terms that are proportional to thermal fluctuations Δx_{th}^4, quantum terms are suppressed by a factor $L^4/\Delta x_{th}^4 = (\hbar\omega_0/(k_BT))^2$. For current AFM designs and at room temperature, this is only about 10^{-15}, but for a tenfold increased resonance frequency and cooled to liquid helium temperatures this ratio could be increased to 10^{-8}.

To separate quantum fluctuations from thermal noise in AFM, we propose to adjust the phase of the driving force in the following way. We start with the observation that, if a term proportional to L^4 appears together with Δx_{th}^4 in one algebraic expression, it is not possible to separate these two terms. This applies to the first and third term inside the square brackets in Eq. (14). Hence, the only quantum term that can potentially be separated is the term proportional to $\sin[2\omega_0(t - t')]$.

To isolate this term, we first note that the first term in square brackets is constant, while the other two terms are oscillating at frequency $2\omega_0$. Hence, the first term can be eliminated through spectral analysis.

To eliminate the second classical term, which is proportional to $\cos[2\omega_0(t - t')]$, we note that the exponential factor in Eq. (14) suppresses the integrand unless the tip is close to the sample, i.e., when $\cos(\omega_0t' + \phi_1) \approx -1$, or $\omega_0t' + \phi_1 \approx \pi(2n + 1)$, with $n \in \mathbb{Z}$. This is a direct consequence of F_{dis} decreasing exponentially with the distance from the surface.

Let us now for simplicity assume that we observe the signal periodically at times t that are multiples of the AFM period, $\omega_0t = 2\pi m$ with $m \in \mathbb{Z}$. We then have $\cos[2\omega_0(t - t')] = \cos(2\omega_0t')$ or, when the tip is close to the surface, $\cos[2\omega_0(t - t')] \approx \cos[2\pi(2n + 1) - 2\phi_1] = \cos(2\phi_1)$. Hence, if we set $\phi_1 = \frac{\pi}{4} + n'\frac{\pi}{2}$, with $n' \in \mathbb{Z}$, we ensure that $\cos[2\omega_0(t - t')] \approx 0$ when the tip is close to the surface. As a consequence, the thermal noise contribution will be strongly suppressed.

The above argument is supported by a numerical evaluation of the cosine integral as a function of ϕ for parameter settings $Q = 400$, $h = 6.7x_\gamma$, and $t = 400\pi/\omega_0$. We found that the integral then varies like $\cos(2\phi_1)$ and indeed vanishes for specific choices of the driving force's phase. If the signal is monitored with period $1/f_0$ at other times t, the phase ϕ_1 of the driving force can be adjusted so that the thermal signal is suppressed as well.

VII. CONCLUSION

We have proposed a driving scheme to increase the interaction time between tip and sample in intermodulation AFM. The tip is described as a stochastic system that can exhibit fluctuations. We derived a set of coupled dynamical equations for probability moments, which have some similarity to the Bogoliubov-Born-Green-Kirkwood-Yvon hierarchy in statistical mechanics [48]. The solution to these equations enables us to reconstruct the tip's phase-space probability distribution.

We use the driving scheme to investigate the generation of squeezing in the classical phase space of the tip. We predict that strong position squeezing is possible if the tip is in close contact with the surface, and if the phases of the two frequency components in intermodulation AFM are chosen appropriately. In the weakly interacting van der Waals regime of the tip-surface interaction, momentum squeezing is predominant.

The dissipative part of the surface force has a strong influence on amount and orientation of phase-space squeezing.

To distinguish between classical and quantum effects, we derived the dynamical equations using both a classical Fokker-Planck equation and a quantum master equation. We found that AFM is generally well described by a classical model. Quantum effects tend to be much smaller than thermally induced fluctuations, but it is possible to separate both effects by adjusting the phase of the driving force in dynamic AFM.

A particularly interesting result is that dissipative surface forces can introduce quantum dynamics already at the level of variances, whereas quantum effects induced by a conservative force are tied to third-order (or higher) probability moments. The derivation of our dynamical equations in Appendix B indicates that the reason is a particular feature of the dissipative force. In the model we studied, it is a position-dependent drag force that depends on two noncommuting observables: position and momentum.

We conjecture that similar effects would also occur with other models for dissipative surface forces. For instance, in the hysteretic Johnson-Kendall-Roberts model [35], the surface force changes depending on whether the tip moves towards or away from the sample; i.e., it depends on position and on the sign of the tip's momentum. In a retarded model [38], the dissipative surface force when the tip is at position $x(t)$ depends on an earlier position $x(t - t_r)$, where t_r is the retardation time of the force. In the Heisenberg picture, $x(t)$ and $x(t - t_r)$ are generally noncommuting.

By probing the probability distribution of the tip, one can examine different Fourier components of the surface force, study its fluctuations, and enhance specific effects, similar to methods used in nonlinear optics. Future work may address the question of whether our driving scheme may also be helpful to measure magnetic surface forces, or if the separation scheme for quantum effects could be useful to isolate specific classical effects as well.

APPENDIX A: CLASSICAL DERIVATION OF DYNAMICAL EQUATIONS BASED ON THE FOKKER-PLANCK EQUATION

For a position-independent drag force $-\gamma_Q p$, the Fokker-Planck equation [49,50] for a classical phase-space probability distribution $f(x, p, t)$ can be written as

$$\partial_t f = -\frac{p}{M}\partial_x f - \partial_p\{[F(x, t) - \gamma_Q p]f\} + \frac{g}{2}\partial_p^2 f, \quad (A1)$$

with $g = 2M\gamma_Q k_BT$. The mean value of a classical observable $A(x, p, t)$, where we admit an explicit time dependence, is given by

$$\langle A \rangle = \int dx\, dp\, f(x, p, t)A(x, p, t). \quad (A2)$$

As above, we use the notation $\bar{x}(t) := \langle x \rangle$ and $\bar{p}(t) := \langle p \rangle$. The time derivative of a mean value can be expressed as

$$\frac{d}{dt}\langle A \rangle = \langle \partial_t A \rangle + \frac{1}{M}\langle p\partial_x A \rangle + \langle (F - \gamma_Q p)\partial_p A \rangle$$
$$+ M\gamma_Q k_B T \langle \partial_p^2 A \rangle. \tag{A3}$$

To add a position-dependent drag force $-\gamma(x)p$, we start with the Langevin equation for such a force:

$$\dot{x} = \frac{p}{M}, \tag{A4}$$

$$\dot{p} = -\gamma(x)p + \zeta, \tag{A5}$$

where ζ is a noise force. We assume δ-correlated noise, for which $\langle \zeta(t) \rangle = 0$ and $\langle \zeta(t)\zeta(t') \rangle = g(t)\delta(t - t')$. The unknown function $g(t)$ can be found using the solution for the momentum:

$$p(t) = p(0)e^{-\bar{\Gamma}(t)} + \int_0^t dt' \, e^{-\bar{\Gamma}(t)+\bar{\Gamma}(t')}\zeta(t'), \tag{A6}$$

$$\bar{\Gamma}(t) = \int_0^t dt' \, \gamma(x(t')). \tag{A7}$$

The mean kinetic energy of the particle is given by $E = \langle p^2 \rangle/(2M)$. For large times, for which $e^{-\bar{\Gamma}(t)} \approx 0$, the particle should reach its equilibrium energy $E = \frac{1}{2}k_B T$. Hence,

$$Mk_B T = \int_0^t dt' \int_0^t dt'' \, e^{-2\bar{\Gamma}(t)+\bar{\Gamma}(t')+\bar{\Gamma}(t'')}\langle \zeta(t')\zeta(t'') \rangle \tag{A8}$$

$$= \int_0^t dt' \, e^{-2\bar{\Gamma}(t)+2\bar{\Gamma}(t')}g(t') \tag{A9}$$

$$= \int_0^t d\tau \, e^{-2\bar{\Gamma}(t)+2\bar{\Gamma}(t-\tau)}g(t-\tau). \tag{A10}$$

If the particle does not move too far during the relaxation process, we can use the approximation $g(t - \tau) \approx g(t)$ and $\bar{\Gamma}(t - \tau) \approx \bar{\Gamma}(t) - \tau\gamma(x(t))$. We can also extend the integra-

tion interval to infinity. We then obtain

$$Mk_B T \approx \frac{g(t)}{2\gamma(x(t))}. \tag{A11}$$

This implies that the factor g takes the same form as for the constant drag force, with γ_Q replaced by $\gamma(x(t))$. This is the approximation we will use below, but we emphasize that this is model dependent. For instance, if we use instead the approximation $g(t - \tau) \approx g(t) - \tau\dot{g}(t)$, we instead obtain the equation

$$Mk_B T \approx \frac{g(t)}{2\gamma(x(t))} - \frac{\dot{g}(t)}{4\gamma^2(x(t))}, \tag{A12}$$

which has the solution

$$g(t) \approx \frac{p_{th}^2}{2}e^{2\int_0^t \gamma(x(t'))dt'}\left\{ \gamma(0) - 2\int_0^t dt'' \, \gamma^2(x(t'')) \right.$$
$$\left. \times \, e^{-2\int_0^{t''} \gamma(x(t'))dt'} \right\}. \tag{A13}$$

Obviously, the precise form of $g(t)$ is difficult to find in a classical model. However, with the simple approximation, we obtain a reasonable agreement with the quantum model. Putting everything together, we obtain the Fokker-Planck equation

$$\frac{d}{dt}\langle A \rangle = \langle \partial_t A \rangle + \frac{1}{M}\langle p\partial_x A \rangle + \langle \{F - [\gamma_Q + \gamma(x)]p\} \, \partial_p A \rangle$$
$$+ Mk_B T \langle [\gamma_Q + \gamma(x)]\partial_p^2 A \rangle. \tag{A14}$$

To derive the classical equations of motion for the correlation functions (5), we consider observables of the form $A = (x - \bar{x})^n(p - \bar{p})^m$, so that

$$\langle \partial_t A \rangle = -n\dot{\bar{x}}\Delta_{n-1,m} - m\dot{\bar{p}}\Delta_{n,m-1} \tag{A15}$$

$$= -n\frac{\bar{p}}{M}\Delta_{n-1,m} - m\langle F - [\gamma_Q + \gamma(x)]p \rangle \Delta_{n,m-1}, \tag{A16}$$

$$\langle p\partial_x A \rangle = n(\bar{p}\Delta_{n-1,m} + \Delta_{n-1,m+1}), \tag{A17}$$

$$\langle \partial_p^2 A \rangle = m(m-1)\Delta_{n,m-2}. \tag{A18}$$

We then obtain

$$\dot{\Delta}_{n,m} = \frac{n}{M}\Delta_{n-1,m+1} - m\gamma_Q\Delta_{n,m} + m\{\langle F - \gamma(x)p(x-\bar{x})^n(p-\bar{p})^{m-1} \rangle - \langle F - \gamma(x)p \rangle \Delta_{n,m-1}\}$$
$$+ Mk_B Tm(m-1)\{\gamma_Q\Delta_{n,m-2} + \langle \gamma(x)(x-\bar{x})^n(p-\bar{p})^{m-2} \rangle\}. \tag{A19}$$

To obtain a closed set of coupled dynamical equations, we assume that uncertainties in position and momentum in the tip motion will remain small, and the tip remains localized. If the forces acting on the system vary little across the extension of the probability distribution, we can expand $F(x)$ and $\gamma(x)$ in a Taylor series around mean position and momentum:

$$F(x) \approx \sum_{n=1}^{n_{max}} \frac{F^{(n)}(\bar{x})}{n!}(x - \bar{x})^n, \tag{A20}$$

$$\gamma(x) \approx \sum_{n=1}^{n_{max}} \frac{\gamma^{(n)}(\bar{x})}{n!}(x - \bar{x})^n. \tag{A21}$$

Applying this approximation to Eq. (A19) leads to

$$
\dot{\Delta}_{n,m} \approx \frac{n}{M}\Delta_{n-1,m+1} - m\gamma_Q\Delta_{n,m} + Mk_BTm(m-1)\left\{\gamma_Q\Delta_{n,m-2} + \sum_{l=0}^{l_{\max}}\frac{\gamma^{(l)}(\bar{x})}{l!}\Delta_{n+l,m-2}\right\}
$$

$$
+ m\sum_{l=0}^{l_{\max}}\frac{1}{l!}\left\{\left[F^{(l)}(\bar{x}) - \gamma^{(l)}(\bar{x})\bar{p}\right](\Delta_{n+l,m-1} - \Delta_{l,0}\Delta_{n,m-1}) - \gamma^{(l)}(\bar{x})(\Delta_{n+l,m} - \Delta_{l,1}\Delta_{n,m-1})\right\}, \qquad \text{(A22)}
$$

which corresponds to the classical part ($\hbar \to 0$) of the set of dynamical equations (B26)–(B34).

APPENDIX B: DERIVATION OF DYNAMICAL EQUATIONS FROM A QUANTUM LINDBLAD MASTER EQUATION

To describe the cantilever as a quantum system, we model it as a one-dimensional quantum harmonic oscillator of mass M that moves in a potential $V(\hat{x})$ and is subject to noise. The density matrix ρ obeys the master equation in Lindblad form [51]:

$$
\dot{\rho} = -\frac{i}{\hbar}[\hat{H}, \rho] - \sum_k(\hat{J}_k^\dagger\hat{J}_k\rho + \rho\hat{J}_k^\dagger\hat{J}_k - 2\hat{J}_k\rho\hat{J}_k^\dagger), \quad \text{(B1)}
$$

$$
\hat{H} = \frac{\hat{p}^2}{2M} + V(\hat{x}), \qquad \text{(B2)}
$$

where $\hat{J}_k$ are jump operators. Force

$$
F(\hat{x}) = -\nabla V \quad = -k\hat{x} + F_{\text{dr}}(t) + F_{\text{SF}}(\hat{x}) \qquad \text{(B3)}
$$

contains all conservative forces that act on the cantilever. This includes the elastic force $-kx$ of the cantilever itself, the homogeneous two-frequency driving force $F_{\text{dr}}(t)$, and the conservative part F_{SF} of the force exerted by the sample surface. The time evolution of the expectation value of an operator $\hat{A}(t)$, for which we admit an explicit time dependence, is given by

$$
\frac{d}{dt}\langle A\rangle = \langle\partial_t\hat{A}\rangle - \frac{i}{\hbar}\langle[\hat{A}, \hat{H}]\rangle - \sum_k\left\langle[\hat{A}, \hat{J}_k^\dagger]\hat{J}_k + \hat{J}_k^\dagger[\hat{J}_k, \hat{A}]\right\rangle.
$$
$$
\text{(B4)}
$$

Our goal is to derive the equations of motion for mean position $\bar{x}(t) = \langle\hat{x}\rangle$, mean momentum $\bar{p}(t) = \langle\hat{p}\rangle$, as well as their variances Δx and Δp. We define a family of symmetric correlation functions $\Delta_{n,m} = \langle\hat{\Delta}_{n,m}\rangle$, with

$$
\hat{\Delta}_{n,m} = \tfrac{1}{2}(\delta\hat{x}^n\delta\hat{p}^m + \delta\hat{p}^m\delta\hat{x}^n), \quad \text{(B5)}
$$

$$
\delta\hat{x} = \hat{x} - \bar{x}, \qquad \text{(B6)}
$$

$$
\delta\hat{p} = \hat{p} - \bar{p}. \qquad \text{(B7)}
$$

There are two prominent noise sources: (i) the damping force due to the finite quality factor Q of the cantilever and (ii) the dissipative force associated with the surface interaction. Damping of the cantilever can be modeled by adding a force $F_Q = -\gamma_Q p$ with damping constant $\gamma_Q = \frac{\omega_0}{Q}$ [39]. In open quantum systems, such a friction force is described through a Caldeira-Leggett model [22] in Lindblad form [see Eq. (5.117) of Ref. [52], for instance]. In this model, the jump

operator takes the form

$$
\hat{J}_Q = \frac{\sqrt{\gamma_Q}}{2}\left(\frac{p_{\text{th}}}{\hbar}\hat{x} + \frac{i}{p_{\text{th}}}\hat{p}\right), \quad \text{(B8)}
$$

and the Hamiltonian is modified by adding a term

$$
\hat{H}_Q = \frac{\gamma_Q}{4}(\hat{x}\hat{p} + \hat{p}\hat{x}). \qquad \text{(B9)}
$$

Here, $p_{\text{th}} = 2\sqrt{Mk_BT}$ corresponds to the momentum uncertainty in thermal equilibrium. Putting this together, the full action of the Caldeira-Leggett model can be written in the form of a superoperator:

$$
\mathcal{L}_Q\hat{A} = -\frac{i}{\hbar}[\hat{A}, \hat{H}_Q] - [\hat{A}, \hat{J}_Q^\dagger]\hat{J}_Q - \hat{J}_Q^\dagger[\hat{J}_Q, \hat{A}] \quad \text{(B10)}
$$

$$
= -\frac{\gamma_Q}{4p_{\text{th}}^2}[\hat{p}, [\hat{p}, \hat{A}]] - \frac{\gamma_Q p_{\text{th}}^2}{4\hbar^2}[\hat{x}, [\hat{x}, \hat{A}]]
$$

$$
- \frac{i\gamma_Q}{2\hbar}\left([\hat{A}, \hat{x}]\hat{p} + \hat{p}[\hat{A}, \hat{x}]\right). \qquad \text{(B11)}
$$

To describe the dissipative part of the surface-tip interaction, we adopt the model of Ref. [39], where the dissipative part takes the form of a drag force that depends on the distance from the sample, $F_{\text{dis}} = -p\gamma(x)$. For most analytical calculations, we will keep the position-dependent dissipation rate $\gamma(x)$ general. However, for numerical evaluations, we will follow Ref. [39] and use an exponential-decay model:

$$
\gamma(x) = \gamma_0\exp\left(-\frac{x+h}{x_\gamma}\right), \qquad \text{(B12)}
$$

where γ_0 is the dissipation rate at the sample surface and x_γ is the length scale on which the dissipative force drops off. In a quantum treatment, $\dot{x}$ has to be replaced by $\hat{p}/m$. One also has to write the operator product in a symmetric way to ensure that the force operator is Hermitian. We therefore seek to generate a dissipative force operator of the form

$$
\hat{F}_{\text{dis}} = -\tfrac{1}{2}[\hat{p}\gamma(\hat{x}) + \gamma(\hat{x})\hat{p}]. \qquad \text{(B13)}
$$

We remark that this reduces to the previous case for $\gamma(x) = \gamma_Q$. We found that it is possible to describe this process through a Lindblad master equation with

$$
\hat{J}_{\text{dis}} = \frac{p_{\text{th}}\sqrt{\tau_0}}{4\hbar}\Gamma(\hat{x}) + \frac{i}{p_{\text{th}}\sqrt{\tau_0}}\hat{p}, \qquad \text{(B14)}
$$

$$
\hat{H}_{\text{dis}} = \tfrac{1}{4}[\hat{p}\Gamma(\hat{x}) + \Gamma(\hat{x})\hat{p}], \qquad \text{(B15)}
$$

where $\Gamma(x)$ is the antiderivative of $\gamma(x)$ and τ_0 is a time scale that will be discussed below. Note that τ_0 may be a function of time. We can then again describe the full action of the

dissipative force in terms of a superoperator:

$$\mathcal{L}_{\text{dis}}\hat{A} = -\frac{i}{\hbar}[\hat{A}, \hat{H}_{\text{dis}}] - [\hat{A}, \hat{J}_{\text{dis}}^\dagger]\hat{J}_{\text{dis}} - \hat{J}_{\text{dis}}^\dagger[\hat{J}_{\text{dis}}, \hat{A}] \quad \text{(B16)}$$

$$= -\frac{1}{\tau_0 p_{\text{th}}^2}[\hat{p}, [\hat{p}, \hat{A}]] - \frac{\tau_0 p_{\text{th}}^2}{16\hbar^2}[\hat{\Gamma}, [\hat{\Gamma}, \hat{A}]]$$

$$- \frac{i}{2\hbar}\left([\hat{A}, \hat{\Gamma}]\hat{p} + \hat{p}[\hat{A}, \hat{\Gamma}]\right). \quad \text{(B17)}$$

We now have to evaluate the equations of motion,

$$\frac{d}{dt}\langle A \rangle = \langle \partial_t \hat{A} \rangle - \frac{i}{\hbar}\langle [\hat{A}, \hat{H}]\rangle + \langle \mathcal{L}_Q \hat{A} + \mathcal{L}_{\text{dis}}\hat{A}\rangle, \quad \text{(B18)}$$

for the correlation functions (B5), which include an explicit time dependence in their definition through $\bar{x}(t)$ and $\bar{p}(t)$. We start with mean position and momentum, which obey

$$\dot{\bar{x}} = \frac{\bar{p}}{M}, \quad \text{(B19)}$$

$$\dot{\bar{p}} = \langle \hat{F}_{\text{tot}} \rangle - \gamma_Q \bar{p}, \quad \text{(B20)}$$

where a dot denotes the time derivative d/dt, and $\hat{F}_{\text{tot}} = F(\hat{x}) + \hat{F}_{\text{dis}}$. For the correlation functions, we find

$$\dot{\Delta}_{n,m} = \frac{n}{M}\Delta_{n-1,m+1} - \frac{i\hbar}{4M}n(n-1)\langle[\delta\hat{x}^{n-2}, \delta\hat{p}^m]\rangle + \frac{i}{2\hbar}\langle\delta\hat{x}^n[V, \delta\hat{p}^m] + [V, \delta\hat{p}^m]\delta\hat{x}^n\rangle - m\langle\hat{F}_{\text{tot}}\rangle\Delta_{n,m-1}$$

$$- m\gamma_Q\Delta_{n,m} + \frac{\gamma_Q p_{\text{th}}^2}{4}m(m-1)\Delta_{n,m-2} + \frac{\hbar^2}{4p_{\text{th}}^2}\left(\gamma_Q + \frac{4}{\tau_0}\right)n(n-1)\Delta_{n-2,m}$$

$$+ \frac{i\hbar\gamma_Q}{4}nm\langle[\delta\hat{x}^{n-1}, \delta\hat{p}^{m-1}]\rangle - \frac{\tau_0 p_{\text{th}}^2}{16\hbar^2}\langle[\hat{\Gamma}, [\hat{\Gamma}, \hat{\Delta}_{n,m}]]\rangle + \frac{i}{2\hbar}\langle[\hat{\Gamma}, \hat{\Delta}_{n,m}]\hat{p} + \hat{p}[\hat{\Gamma}, \hat{\Delta}_{n,m}]\rangle. \quad \text{(B21)}$$

This result is exact, but its usefulness hinges on our ability to evaluate commutators of powers of $\hat{p}$ and functions of $\hat{x}$. This is accomplished in Appendix F. Result (F16) states that a commutator of the form $[V(\hat{x}), \hat{p}^n]$ can be written in terms of Euler polynomials with an argument that contains $\hat{p}$ and the derivative operator $\partial/\partial\hat{x}$, which acts on $V(\hat{x})$. In particular, if the function $V(\hat{x})$ is a polynomial, the commutator corresponds to

$$\langle[\delta\hat{x}^m, \delta\hat{p}^n]\rangle = i\sum_{l=1}^{\min(m,n)}C_{n,m,l}\hbar^l\Delta_{m-l,n-l}, \quad \text{(B22)}$$

where coefficients $C_{n,m,l}$ are defined through Eq. (F17). Hence, it can be expressed in terms of correlation functions (B5). However, potential $V(\hat{x})$ and factor $\Gamma(\hat{x})$ will generally not be of a polynomial form, so that the equations of motion will not form a closed set of equations. It is therefore necessary to make approximations.

With localization approximation (A20), the expectation value of all quantities appearing in the equations of motion

can be expressed in terms of correlation functions (B5). For instance,

$$\langle F(\hat{x})\rangle = \sum_{n=1}^{n_{\text{max}}}\frac{F^{(n)}(\bar{x})}{n!}\Delta_{n,0}, \quad \text{(B23)}$$

$$\langle F_{\text{dis}}(\hat{x})\rangle = -\frac{1}{2}\sum_{n=1}^{n_{\text{max}}}\frac{\gamma^{(n)}(\bar{x})}{n!}\langle\hat{p}(\hat{x}-\bar{x})^n + (\hat{x}-\bar{x})^n\hat{p}\rangle \quad \text{(B24)}$$

$$= -\sum_{n=1}^{n_{\text{max}}}\frac{\gamma^{(n)}(\bar{x})}{n!}(\Delta_{n,1} + \bar{p}\Delta_{n,0}). \quad \text{(B25)}$$

We note that elastic force $-kx$, cantilever damping γ_Q, and homogeneous driving force $F_{\text{dr}}(t)$ are taken into account exactly. This is because their Taylor series terminate after the first term, so that the above approximation leaves these forces unaffected.

Using similar expansions up to third order ($n_{\text{max}} = 3$) for all terms in the equation of motions, and treating terms $\Delta_{n,m}$ as of order ϵ^{n+m} in the deviations from mean values, we arrive at the following equations:

$$\frac{d\bar{x}}{dt} = \frac{\bar{p}}{M}, \quad \text{(B26)}$$

$$\frac{d\bar{p}}{dt} : \text{ see Eq. (7)}, \quad \text{(B27)}$$

$$\frac{d\Delta_{2,0}}{dt} = \frac{2}{M}\Delta_{1,1} + \frac{\hbar^2}{2p_{\text{th}}^2}\left(\gamma_Q + \frac{4}{\tau_0}\right), \quad \text{(B28)}$$

$$\frac{d\Delta_{1,1}}{dt} = \frac{1}{M}\Delta_{0,2} - (\gamma_Q + \gamma(\bar{x}))\Delta_{1,1} + \Delta_{2,0}[F'(\bar{x}) - \bar{p}\gamma'(\bar{x})] - \gamma'(\bar{x})\Delta_{2,1} + \frac{1}{2}\Delta_{3,0}[F''(\bar{x}) - \bar{p}\gamma''(\bar{x})], \quad \text{(B29)}$$

$$\frac{d\Delta_{0,2}}{dt} = 2[F'(\bar{x}) - \bar{p}\gamma'(\bar{x})]\Delta_{1,1} - 2\gamma_Q\left(\Delta_{0,2} - \frac{p_{\text{th}}^2}{4}\right) - 2\gamma(\bar{x})\Delta_{0,2} - \frac{\hbar^2}{2}\gamma''(\bar{x}) + [F''(\bar{x}) - \bar{p}\gamma''(\bar{x})]\Delta_{2,1} - 2\gamma'(\bar{x})\Delta_{1,2}$$

$$+ \frac{p_{\text{th}}^2\tau_0}{8}\left[\gamma^2(\bar{x}) + \Delta_{2,0}[\gamma'(\bar{x})^2 + \gamma(\bar{x})\gamma''(\bar{x})] + \left(\gamma'(\bar{x})\gamma''(\bar{x}) + \frac{1}{3}\gamma(\bar{x})\gamma'''(\bar{x})\right)\Delta_{3,0}\right], \quad \text{(B30)}$$

$$\frac{d\Delta_{3,0}}{dt} = \frac{3}{M}\Delta_{2,1}, \tag{B31}$$

$$\frac{d\Delta_{2,1}}{dt} = \frac{2\Delta_{1,2}}{M} - [\gamma_Q + \gamma(\bar{x})]\Delta_{2,1} + \Delta_{3,0}[F'(\bar{x}) - \bar{p}\gamma'(\bar{x})], \tag{B32}$$

$$\frac{d\Delta_{1,2}}{dt} = \frac{\Delta_{0,3}}{M} - 2[\gamma_Q + \gamma(\bar{x})]\Delta_{1,2} + 2\Delta_{2,1}[F'(\bar{x}) - \bar{p}\gamma'(\bar{x})]$$

$$+ \Delta_{2,0}\left(\frac{p_{\text{th}}^2\tau_0}{4}\gamma'(\bar{x})\gamma(\bar{x}) - \hbar^2\gamma'''(\bar{x})\right) - \hbar^2\gamma'(\bar{x}) + \Delta_{3,0}\frac{p_{\text{th}}^2\tau_0}{8}[\gamma(\bar{x})\gamma''(\bar{x}) + \gamma'^2(\bar{x})], \tag{B33}$$

$$\frac{d\Delta_{0,3}}{dt} = -3\Delta_{0,3}[\gamma_Q + \gamma(\bar{x})] + 3\Delta_{1,2}[F'(\bar{x}) - \bar{p}\gamma'(\bar{x})] + \frac{1}{2}\hbar^2[F''(\bar{x}) - \bar{p}\gamma''(\bar{x})] - 2\hbar^2\Delta_{1,1}\gamma'''(\bar{x})$$

$$+ \frac{3}{8}\tau_0 p_{\text{th}}^2\{2\Delta_{1,1}\gamma(\bar{x})\gamma'(\bar{x}) + \Delta_{2,1}[\gamma'(\bar{x})^2 + \gamma(\bar{x})\gamma''(\bar{x})]\}. \tag{B34}$$

These equations represent the main theoretical result of this paper. We have verified that, except for two types of terms, they agree with the corresponding equations for a classical model based on the Fokker-Planck equation, which is derived in Appendix A. The two types of terms in which the two models differ are (i) terms that depend on $\hbar$ and (ii) terms that depend on derivatives of $\gamma(x)$. We will now discuss these differences.

Terms involving $\hbar$ correspond to genuine quantum dynamics. The first occurrence in Eq. (B28) corresponds to the position uncertainty relation $\Delta x \sim \hbar/\Delta p$ if the momentum uncertainty is equal to the thermal momentum p_{th}. The only other occurrence in the equations for the second-order variances depends on the curvature $\gamma''(\bar{x})$ of the dissipative part of the surface force. It is interesting to observe that applying a position-dependent dissipative force may be an effective way to observe differences between classical and quantum dynamics of a localized system. By comparison, quantum dynamics induced by the conservative part of the force only appear in the dynamical equation for the momentum skewness $\Delta_{0,3}$.

We now turn to terms of type (ii) and the role of time scale τ_0. We start by considering the stationary solution for the case that $F = 0 = \gamma_Q$. The equations of motion then have a quasistationary solution of the form $\bar{p} = 0$, $\bar{x}$ constant, as well as

$$\Delta p = \frac{p_{\text{th}}}{4}\sqrt{\tau_0\gamma(\bar{x})}, \tag{B35}$$

$$\Delta_{1,1} = \frac{p_{\text{th}}^2\tau_0}{16m}, \tag{B36}$$

$$\Delta x = \sqrt{t\left(\frac{p_{\text{th}}^2\tau_0}{8M^2} + \frac{2\hbar^2}{p_{\text{th}}^2\tau_0}\right)}, \tag{B37}$$

and $\Delta_{n,m} = 0$ for the third-order correlation functions. If we want to ensure that the momentum uncertainty Δp is equal to $p_{\text{th}}/2$ in this case, we have to set $\tau_0 = 4/\gamma(\bar{x})$.

A second reason why τ_0 should be equal to $4/\gamma(\bar{x})$ is the comparison with the classical Fokker-Planck equation (A22).

In the classical limit ($\hbar = 0$) and for constant $\bar{x}$, the two sets of equations only agree if τ_0 is chosen in this way.

However, even for $\tau_0 = 4/\gamma(\bar{x})$ and in the classical limit, the Fokker-Planck equation differs from the results above if $\gamma(\bar{x}(t))$ varies with $\bar{x}(t)$, and these are the terms of type (ii). In the quantum derivation, these terms are a direct consequence of model (B14) for inhomogeneous quantum dissipative forces. This model appears to be the only one where the jump operator $\hat{J}_{\text{dis}}$ is linear in the momentum operator. Hence, as long as the dissipative force is created by systems that are Markovian (this is the underlying assumption of the Lindblad form), the derivative terms are needed for consistency. Furthermore, as discussed in Appendix A, the absence of derivatives of $\gamma(x)$ in the classical equations (A22) is merely a consequence of an approximation. A refined Fokker-Planck model would likely generate similar terms, so that we believe that the presence of type (ii) terms is physically well justified.

APPENDIX C: RECONSTRUCTING A CLASSICAL PROBABILITY DISTRIBUTION FROM CORRELATION FUNCTIONS

We consider an N-dimensional phase space $\mathbb{R}^N$ with $\boldsymbol{r}$ denoting an element of this space. In our case, $\boldsymbol{r} = (x, p)$ is the two-dimensional phase space of a particle with one degree of freedom. A probability distribution $\rho(\boldsymbol{r})$ is a real positive function that is normalized to unity:

$$1 = \int d^N r \, \rho(\boldsymbol{r}). \tag{C1}$$

The nth moment around a point $\bar{\boldsymbol{r}} \in \mathbb{R}^N$ is defined as

$$\mu_n = \int d^N r \, (\boldsymbol{r} - \bar{\boldsymbol{r}})^n \rho(\boldsymbol{r}). \tag{C2}$$

Here and in the following, we will employ a multi-index notation: for a tuple $n = (n_1, \cdots, n_N)$ of k integer numbers, we set

$$|n| = n_1 + n_2 + \cdots + n_N, \tag{C3}$$

$$n! = n_1! \, n_2! \cdots n_N!, \tag{C4}$$

$$\boldsymbol{r}^n = r_1^{n_1} r_2^{n_2} \cdots r_N^{n_N}, \tag{C5}$$

$$D^n f(\boldsymbol{r}) = \frac{\partial^{|n|} f}{\partial_1^{n_1} \cdots \partial_N^{n_N}}. \tag{C6}$$

In this Appendix, we answer the following question: Given the moments μ_n of a probability distribution $\rho(\boldsymbol{r})$, can we reconstruct ρ?

To describe asymmetric probability distributions, Azzalini and Valle [43] introduced a multivariable extension of the skew-normal distribution of the form

$$\rho(\boldsymbol{r}) = \rho_0(\boldsymbol{r})\Phi(\boldsymbol{r}), \tag{C7}$$

where ρ_0 corresponds to a Gaussian distribution (9), with C a positive symmetric $N \times N$ matrix.

In Ref. [43], Φ is a specific function, but we consider Φ as an unknown function that needs to be reconstructed using the moments. We denote the moments of the Gaussian probability distribution by $\mu_n^{(0)}$ and assume that Φ possesses a Taylor expansion around $\bar{\boldsymbol{r}}$, which in multi-index notation takes the form

$$\Phi(\boldsymbol{r}) = \sum_k \frac{1}{k!} D^k \Phi(\bar{\boldsymbol{r}}) (\boldsymbol{r} - \bar{\boldsymbol{r}})^k. \tag{C8}$$

We then can express the moments around point $\bar{\boldsymbol{r}}$ as

$$\mu_n = \int d^N r \, (\boldsymbol{r} - \bar{\boldsymbol{r}})^n \, \rho_0(\boldsymbol{r}) \sum_k \frac{1}{k!} D^k \Phi(\bar{\boldsymbol{r}}) (\boldsymbol{r} - \bar{\boldsymbol{r}})^k \tag{C9}$$

$$= \sum_k \frac{1}{k!} D^k \Phi(\bar{\boldsymbol{r}}) \mu_{n+k}^{(0)}. \tag{C10}$$

This corresponds to a set of linear equations that enable us to express, up to a given order, $D^k \Phi(\bar{\boldsymbol{r}})$ in terms of μ_n. Of particular interest is the case when $\bar{\boldsymbol{r}}$ corresponds to the measured mean value. In this situation, moments μ_k directly correspond to the correlation function $\Delta_{n,m}$ that we study in the main text.

For a Gaussian distribution, all odd moments vanish, $\mu_{2n+1}^{(0)} = 0$. The even moments are given by

$$\mu_{i_1,i_2,\cdots,i_{2n}}^{(0)} = \int d^N r \, \rho_0(\boldsymbol{r})(\boldsymbol{r} - \bar{\boldsymbol{r}})_{i_1} \cdots (\boldsymbol{r} - \bar{\boldsymbol{r}})_{i_{2n}} \tag{C11}$$

$$= \frac{1}{(2\pi)^{N/2}|C|^{\frac{1}{2}}} \int d^N x \, x_{i_1} \cdots x_{i_{2n}} e^{-\frac{1}{2}\boldsymbol{x}^T \cdot C^{-1} \cdot \boldsymbol{x}} \tag{C12}$$

$$= \frac{1}{2^n n!} \sum_p C_{i_{p(1)} i_{p(2)}} \cdots C_{i_{p(2n-1)} i_{p(2n)}}, \tag{C13}$$

where the sum runs over all permutations p of the indices $i_1, \cdots i_{2n}$. Explicitly, moments 2, 4, and 6 are given by

$$\mu_{i_1,i_2}^{(0)} = C_{i_1,i_2}, \tag{C14}$$

$$\mu_{i_1,i_2,i_3,i_4}^{(0)} = C_{i_1,i_4}C_{i_2,i_3} + C_{i_1,i_3}C_{i_2,i_4} + C_{i_1,i_2}C_{i_3,i_4}, \tag{C15}$$

$$\begin{aligned}
\mu_{i_1,i_2,i_3,i_4,i_5,i_6}^{(0)} &= C_{i_1,i_6}C_{i_2,i_5}C_{i_3,i_4} + C_{i_1,i_5}C_{i_2,i_6}C_{i_3,i_4} + C_{i_1,i_2}C_{i_5,i_6}C_{i_3,i_4} + C_{i_1,i_6}C_{i_2,i_4}C_{i_3,i_5} + C_{i_1,i_4}C_{i_2,i_6}C_{i_3,i_5} \\
&\quad + C_{i_1,i_5}C_{i_2,i_4}C_{i_3,i_6} + C_{i_1,i_4}C_{i_2,i_5}C_{i_3,i_6} + C_{i_1,i_6}C_{i_2,i_3}C_{i_4,i_5} + C_{i_1,i_3}C_{i_2,i_6}C_{i_4,i_5} + C_{i_1,i_2}C_{i_3,i_6}C_{i_4,i_5} \\
&\quad + C_{i_1,i_5}C_{i_2,i_3}C_{i_4,i_6} + C_{i_1,i_3}C_{i_2,i_5}C_{i_4,i_6} + C_{i_1,i_2}C_{i_3,i_5}C_{i_4,i_6} + C_{i_1,i_4}C_{i_2,i_3}C_{i_5,i_6} + C_{i_1,i_3}C_{i_2,i_4}C_{i_5,i_6}.
\end{aligned} \tag{C16}$$

We now use these results and Eq. (C10) to find the Taylor coefficients $D^k \Phi(\bar{\boldsymbol{r}})$ up to order $k = 3$. We start by writing down explicitly the first four moments. $\mu_0 = 1$ expresses normalization of probability:

$$1 = \mu_0 \tag{C17}$$

$$= \Phi(\bar{\boldsymbol{r}})\mu_0^{(0)} + \frac{1}{(2)!}D^2\Phi(\bar{\boldsymbol{r}})\mu_2^{(0)} \tag{C18}$$

$$= \Phi(\bar{\boldsymbol{r}}) + \sum_{i_1,i_2} \frac{1}{(i_1 i_2)!}[\partial_{i_1}\partial_{i_2}\Phi(\bar{\boldsymbol{r}})]C_{i_1 i_2}. \tag{C19}$$

Here, notation $(i_1 i_2)!$ is a multi-index notation that is equal to 2! if both indices are equal, and 1 otherwise. Below, we will also use $(i_1 i_2 i_3)!$ equal to 3! for all three indices equal, 2! if only two are equal, and 1 otherwise.

Since $\bar{\boldsymbol{r}}$ is equal to the mean position, $\mu_1 = 0$ by definition. Hence, the second equation becomes

$$0 = D^1\Phi \, \mu_2^{(0)} + \frac{1}{(3)!}D^3\Phi \, \mu_4^{(0)}, \tag{C20}$$

or with explicit indices,

$$0 = \sum_{i_2}(\partial_{i_2}\Phi)\mu_{i_1 i_2}^{(0)} + \sum_{i_2,i_3,i_4} \frac{1}{(i_2 i_3 i_4)!}(\partial_{i_2}\partial_{i_3}\partial_{i_4}\Phi)\mu_{i_1 i_2 i_3 i_4}^{(0)} \tag{C21}$$

$$= \sum_{i_2}(\partial_{i_2}\Phi)C_{i_1 i_2} + \sum_{i_2,i_3,i_4} \frac{1}{(i_2 i_3 i_4)!}(\partial_{i_2}\partial_{i_3}\partial_{i_4}\Phi)(C_{i_1 i_4}C_{i_2 i_3}$$

$$+ C_{i_1 i_3}C_{i_2 i_4} + C_{i_1 i_2}C_{i_3 i_4}). \tag{C22}$$

Since the multifactorial and the derivatives of Φ are totally symmetric under exchange of indices i_2, i_3, and i_4, we can reduce the second factor to a sum over a single term:

$$0 = \sum_{i_2}(\partial_{i_2}\Phi)C_{i_1 i_2} + 3\sum_{i_2,i_3,i_4} \frac{1}{(i_2 i_3 i_4)!}(\partial_{i_2}\partial_{i_3}\partial_{i_4}\Phi)C_{i_1 i_4}C_{i_2 i_3}. \tag{C23}$$

Multiplying this with $(C^{-1})_{ii_1}$ and summing over i_1 yields

$$\partial_i\Phi(\bar{\boldsymbol{r}}) = -3\sum_{i_2,i_3} \frac{1}{(i \, i_2 i_3)!}(\partial_i\partial_{i_2}\partial_{i_3}\Phi)C_{i_2 i_3}. \tag{C24}$$

The second-order moment equals the correlation matrix, $\mu_{i_1 i_2} = \langle (\boldsymbol{r} - \bar{\boldsymbol{r}})_{i_1} (\boldsymbol{r} - \bar{\boldsymbol{r}})_{i_2} \rangle$. The equation for this moment reads

$$\mu_2 = \Phi(\bar{\boldsymbol{r}}) \mu_2^{(0)} + \frac{1}{(2)!} D^2 \Phi(\bar{\boldsymbol{r}}) \mu_4^{(0)}. \qquad \text{(C25)}$$

Together with Eq. (C18), this provides us with a linear set of equations for the $N^2 + 1$ coefficients $\Phi(\bar{\boldsymbol{r}})$ and $D^2 \Phi(\bar{\boldsymbol{r}})$. This is easy to solve if we pick matrix C in the Gaussian distribution (9) such that $\mu_2^{(0)} = \mu_2$. This is accomplished for the choice $C_{i_1 i_2} = \mu_{i_1 i_2}$. Equations (C18) and (C25) are then easily solved by $\Phi(\bar{\boldsymbol{r}}) = 1$ and $D^2 \Phi(\bar{\boldsymbol{r}}) = 0$.

The equation for the third-order moment is given by

$$\mu_3 = D^1 \Phi \, \mu_4^{(0)} + \frac{1}{(3)!} D^3 \Phi \, \mu_6^{(0)}, \qquad \text{(C26)}$$

or with explicit indices,

$$\mu_{i_1 i_2 i_3} = \sum_{i_4} (\partial_{i_4} \Phi) \mu_{i_1 i_2 i_3 i_4}^{(0)}$$
$$+ \sum_{i_4, i_5, i_6} \frac{1}{(i_4 i_5 i_6)!} (\partial_{i_4} \partial_{i_5} \partial_{i_6} \Phi) \mu_{i_1 i_2 i_3 i_4 i_5 i_6}^{(0)}. \qquad \text{(C27)}$$

We can exploit Eq. (C24) to turn this equation into one that only contains the third-order derivatives $(\partial_{i_4} \partial_{i_5} \partial_{i_6} \Phi)$. The triple sum contains factors like Eq. (C16), which are very lengthy. However, the high degree of symmetry of all factors involved enables us to reduce it to

$$\mu_{i_1 i_2 i_3} = 6 \sum_{i_4, i_5, i_6} \frac{1}{(i_4 i_5 i_6)!} (\partial_{i_4} \partial_{i_5} \partial_{i_6} \Phi) C_{i_1 i_4} C_{i_2 i_5} C_{i_3 i_6}. \qquad \text{(C28)}$$

This equation is easily solved and lets us determine all Taylor coefficients up to order 3:

$$\partial_i \partial_j \partial_k \Phi(\bar{\boldsymbol{r}}) = \frac{(i j k)!}{6} \sum_{i_1, i_2, i_3} \mu_{i_1 i_2 i_3} (C^{-1})_{i \, i_1} (C^{-1})_{j \, i_2} (C^{-1})_{k \, i_3}, \qquad \text{(C29)}$$

$$\partial_i \Phi(\bar{\boldsymbol{r}}) = -\frac{1}{2} \sum_{i_1, i_2, i_3} \mu_{i_1 i_2 i_3} (C^{-1})_{i \, i_1} (C^{-1})_{i_2 \, i_3}. \qquad \text{(C30)}$$

The full expression for $\Phi(\boldsymbol{r})$ is then given by Eq. (11).

Turning to the two-dimensional case that is the subject of this paper, we use correlation matrix (10), with

$$C^{-1} = \sigma_1^{-2} \sigma_2^{-2} \begin{pmatrix} \Delta_{02} & -\Delta_{11} \\ -\Delta_{11} & \Delta_{20} \end{pmatrix}. \qquad \text{(C31)}$$

Matrix C has eigenvectors and eigenvalues

$$\boldsymbol{e}_{\underline{1}} = \frac{1}{\sqrt{2W(W - \Delta_{02} + \Delta_{20})}} \begin{pmatrix} \Delta_{20} - \Delta_{02} + W \\ 2\Delta_{11} \end{pmatrix},$$

$$C \cdot \boldsymbol{e}_{\underline{1}} = \sigma_1^2 \boldsymbol{e}_{\underline{1}} = \frac{1}{2}(\Delta_{20} + \Delta_{02} + W) \boldsymbol{e}_{\underline{1}}, \qquad \text{(C32)}$$

$$\boldsymbol{e}_{\underline{2}} = \frac{1}{\sqrt{2W(W + \Delta_{02} - \Delta_{20})}} \begin{pmatrix} \Delta_{20} - \Delta_{02} - W \\ 2\Delta_{11} \end{pmatrix},$$

$$C \cdot \boldsymbol{e}_{\underline{2}} = \sigma_2^2 \boldsymbol{e}_{\underline{2}} = \frac{1}{2}(\Delta_{20} + \Delta_{02} - W) \boldsymbol{e}_{\underline{2}}, \qquad \text{(C33)}$$

$$W = \sqrt{4\Delta_{11}^2 + (\Delta_{20} - \Delta_{02})^2}. \qquad \text{(C34)}$$

Here, σ_1 and σ_2 are the variances along the directions of the eigenvectors of C. The third-order moment has components $\mu_{111} = \Delta_{30}$, $\mu_{222} = \Delta_{03}$, and $\mu_{112} = \mu_{121} = \mu_{211} = \Delta_{21}$, as well as $\mu_{221} = \mu_{212} = \mu_{122} = \Delta_{12}$. Introducing tensor components

$$T_1^{(1)} = \Delta_{30} + \Delta_{12}, \qquad \text{(C35)}$$

$$T_2^{(1)} = \Delta_{03} + \Delta_{21}, \qquad \text{(C36)}$$

$$T_1^{(3)} = \tfrac{1}{3}\Delta_{30} - \Delta_{12}, \qquad \text{(C37)}$$

$$T_2^{(3)} = -\tfrac{1}{3}\Delta_{03} + \Delta_{21}, \qquad \text{(C38)}$$

we can express function Φ as

$$\Phi(\boldsymbol{r}) = 1 + \boldsymbol{S} \cdot \boldsymbol{R} + \frac{|\boldsymbol{R}|^2}{8} \boldsymbol{T}^{(1)} \cdot \boldsymbol{R}$$
$$+ \frac{1}{8} T_1^{(3)} (R_1^3 - 3R_1 R_2^2) + \frac{1}{8} T_2^{(3)} (3R_2 R_1^2 - R_2^3). \qquad \text{(C39)}$$

In polar coordinates, $R_1 = R \cos \phi$ and $R_2 = R \sin \phi$, tensors $\boldsymbol{T}^{(1)}$ and $\boldsymbol{T}^{(3)}$ describe terms that vary like $\cos \phi$ and $\sin \phi$, or $\cos 3\phi$ and $\sin 3\phi$, respectively. Hence, $\boldsymbol{T}^{(1)}$ describes the direction in which the extended tail of ρ points, while $\boldsymbol{T}^{(3)}$ describes deformations of a triangular shape.

APPENDIX D: NUMERICAL SIMULATIONS

To solve the dynamical equations (B26)–(B34) numerically, we consider a cantilever with a resonance frequency $f_0 = \omega_0/(2\pi) = 300$ kHz, a spring constant of $M\omega_0^2 = 40.0$ N/m, and a quality factor of $Q = 400$. The cantilever starts from its equilibrium position and from thermal equilibrium at room temperature (300 K).

To model the surface force, we follow Platz *et al.* [39] and assume an exponentially decreasing dissipative force $F_{\text{dis}} = -\gamma(x)p$, with $\gamma(x)$ given by Eq. (B12), with $x_\gamma = 1.5$ nm and $2\pi \gamma_0/\omega_0 \approx 0.065$. For the conservative surface force, we employ a modification of the van der Waals–DMT model. In its original form, the DMT force is given by

$$F_{\text{DMT}}(x) = \begin{cases} -\dfrac{HR}{6(a_0 + x + h)^2} & x > -h \\ -\dfrac{HR}{6a_0^2} + \dfrac{4}{3} E^* \sqrt{R}(-h - x)^{\frac{3}{2}} & x < -h \end{cases}, \qquad \text{(D1)}$$

where $H = 3.28 \times 10^{-17} \text{ kg m}^2 \text{ s}^{-2}$ is the Hamaker constant, which is a measure for the van der Waals interaction energy between tip and surface. $R = 10$ nm denotes the tip radius, and $a_0 = 2.7$ nm represents the intermolecular distance. $E^* = 1.5$ GPa is the effective stiffness of the tip-sample system. The piecewise definition of this force makes it unsuitable for our purposes, since derivatives of Eq. (D1) are not well defined at $x = -h$. We therefore employ a modified model, which is continuously

differentiable:

$$F_{\text{SF}}(x) = -\frac{1.15HR}{12}\frac{\left[1 + \tanh\left(\frac{x+h}{L_f}\right)\right]}{L_f^2 + (a_0 + x + h)^2} + \frac{1}{2}\left[1 - \tanh\left(\frac{x+h}{L_f}\right)\right]\left(-\frac{1.15HR}{6(L_f^2 + a_0^2)} + \frac{4}{3}E^*\sqrt{R}[L_f^2 + (h+x)^2]^{\frac{3}{4}}\right). \quad \text{(D2)}$$

Here, $L_f = a_0/4$ controls the smoothness of the transition between van der Waals and surface regions. A plot of model force (D2) and the original DMT model (D1) is shown in Fig. 5.

We have performed a series of numerical simulations of the full dynamical equations (B26)–(B34) with the parameters for the surface-tip interaction as given above. In all simulations, we have considered several special cases.

(1) *Full equations*: The full set of equations (B26)–(B34) is simulated.

(2) *Variance limit*: Only second-order correlation functions Δ_{20}, Δ_{11}, and Δ_{02} are taken into account; third-order variances ($\Delta_{n,m}$ with $n + m = 3$) are set to zero.

(3) *Point-particle limit*: All correlation functions Δ_{nm} are assumed to vanish.

(4) *Reduced dissipative force*: To study the influence of the dissipative force, we have run the simulations in a situation where the dissipative surface force is reduced by a factor of 10^{-3}.

(5) *No quantum terms*: All quantum terms [terms involving $\hbar$ in Eqs. (B26)–(B34)] are set to zero.

In addition, we have performed numerical simulations that include fourth-order correlation functions ($\Delta_{n,m}$ with $n + m = 4$) to verify that these terms can be ignored. These results were affirmative and are not presented in this paper. Since the general validity of our method hinges on the validity of localization approximation (6), the conditions for its validity need to be checked. One way is to increase the order of approximations, and the fact that fourth-order calculations yield the same results as third-order calculations indicates that the conditions are met. Another way to check the validity is to estimate the error in the force. For a third-order calculation, this error can be estimated as $\delta F(x) = \frac{1}{4!}F^{(4)}(x)\Delta x^4$, where Δx is the spatial width of the probability distribution. Even in the most extreme situation [the strongly momentum-squeezed cloud of Fig. 3(c) in the absence of a dissipative force], this error never exceeds 0.01 nN. In the presence of a dissipative surface force [Fig. 3(a)], the error does not exceed 10^{-4} nN.

In agreement with first-order perturbation theory (see Appendix E), we found two general results in our simulations.

(i) If one is only interested in studying mean position and momentum of the cantilever, the point-particle limit is appropriate. Variances only have a small effect on their dynamics.

(ii) For standard AFM parameters, quantum terms can safely be neglected. Since thermal variances are generally several orders of magnitude larger than quantum uncertainties, our results do not support claims in the literature that AFM is quantum limited [53].

The simulation supports the findings that we found in perturbation theory: significant squeezing is only generated when the tip is in contact with the sample.

APPENDIX E: PERTURBATION THEORY OF THE DRIVEN CANTILEVER

If the tip-surface interaction is sufficiently small, the surface forces can be treated as a perturbation. To derive a solution of Eqs. (B26)–(B34) to first order in perturbation theory, we assume that the unperturbed system is initially thermalized, i.e., mean position and momentum follow a stationary trajectory, and the variances correspond to a thermal equilibrium. The full unperturbed solution for driving force (2) is then given by the unperturbed mean position $x_0(t)$ of Eq. (3), unperturbed mean momentum $p_0(t) = M\dot{x}_0$, as well as

$$\Delta x_{\text{th}}^2 := \Delta_{20}^{\text{(no srfc.)}} = \frac{k_B T}{M\omega_0^2}\left[1 + \left(1 + \frac{1}{Q^2}\right)\left(\frac{\hbar\omega_0}{4k_B T}\right)^2\right], \quad \text{(E1)}$$

$$\Delta_{02}^{\text{(no srfc.)}} = Mk_B T\left[1 + \left(\frac{\hbar\omega_0}{4k_B T}\right)^2\right], \quad \text{(E2)}$$

and $\Delta_{n,m} = 0$ otherwise. For a typical cantilever, the ratio of ground-state energy $\hbar\omega_0$ and thermal energy $k_B T$ is on the order of 10^{-8}. Here and in the following, we will therefore neglect terms of order $\hbar^2$ and only keep lowest-order quantum contributions. We will also neglect terms of order Q^{-1} since the quality factor is typically on the order of 10^2. With this approximation, we find the usual result for the thermal uncertainty of a classical oscillator, $\Delta x_{\text{th}} = \sqrt{k_B T/M\omega_0^2}$.

To include the effect of surface forces, we consider the following dimensionless nine-component vector of first-order corrections:

$$\vec{V} = \left(\frac{\Delta_{20}^{(1)}}{L^2}, \frac{\Delta_{11}^{(1)}}{\hbar}, \frac{\Delta_{02}^{(1)}L^2}{\hbar^2}, \frac{\Delta_{30}^{(1)}}{L^3}, \frac{\Delta_{21}^{(1)}L}{L\hbar}, \frac{\Delta_{12}^{(1)}L}{\hbar^2}, \frac{\Delta_{03}^{(1)}L^3}{\hbar^3}, \frac{x^{(1)}}{L}, \frac{p^{(1)}L}{\hbar}\right), \quad \text{(E3)}$$

where a superscript (1) indicates a first-order perturbation term and $L = \sqrt{\hbar/(M\omega_0)}$ is the ground-state width. The perturbative dynamical equations for this vector can be written as

$$\partial_t\vec{V} = M \cdot \vec{V} + \vec{J}, \quad \text{(E4)}$$

with matrix

$$M = \begin{pmatrix} 0 & 2\omega_0 & 0 & 0 & 0 & 0 & 0 & 0 & 0 \\ -\omega_0 & -\gamma_Q & \omega_0 & 0 & 0 & 0 & 0 & 0 & 0 \\ 0 & -2\omega_0 & -2\gamma_Q & 0 & 0 & 0 & 0 & 0 & 0 \\ 0 & 0 & 0 & 0 & 3\omega_0 & 0 & 0 & 0 & 0 \\ 0 & 0 & 0 & -\omega_0 & -\gamma_Q & 2\omega_0 & 0 & 0 & 0 \\ 0 & 0 & 0 & 0 & -2\omega_0 & -2\gamma_Q & \omega_0 & 0 & 0 \\ 0 & 0 & 0 & 0 & 0 & -3\omega_0 & -3\gamma_Q & 0 & 0 \\ 0 & 0 & 0 & 0 & 0 & 0 & 0 & 0 & \omega_0 \\ 0 & 0 & 0 & 0 & 0 & 0 & 0 & -\omega_0 & -\gamma_Q \end{pmatrix}, \tag{E5}$$

and inhomogeneity components $J_4 = J_5 = J_8 = 0$, and

$$J_1 = -\frac{\hbar\gamma(\bar{x})}{8M\omega_0\Delta x_{\text{th}}^2}, \tag{E6}$$

$$J_2 = -\frac{\Delta x_{\text{th}}^2[F_{\text{SF}}'(x_0) - p_0\gamma'(x_0)]}{\hbar} - \frac{\hbar[F_{\text{SF}}'(x_0) - p_0\gamma'(x_0) + M\gamma_Q\gamma(x_0)]}{16M^2\omega_0^2\Delta x_{\text{th}}^2}, \tag{E7}$$

$$J_3 = -\frac{2M\omega_0\Delta x_{\text{th}}^4[\gamma'(x_0)^2 + \gamma(x_0)\gamma''(x_0)]}{\hbar\gamma(x_0)}$$

$$+ \frac{\hbar\{\gamma_Q[F_{\text{SF}}'(x_0) - p_0\gamma'(x_0)] + M\omega_0^2\gamma(x_0)\}}{8M^2\omega_0^3\Delta x_{\text{th}}^2} - \frac{\hbar[\gamma'(x_0)^2 - 3\gamma(x_0)\gamma''(x_0)]}{8M\omega_0\gamma(x_0)}, \tag{E8}$$

$$J_6 = -\frac{4\Delta x_{\text{th}}^4\gamma'(x_0)}{L^3} + L\Delta x_{\text{th}}^2\gamma^{(3)}(x_0) + \frac{3}{4}L\gamma'(x_0), \tag{E9}$$

$$J_7 = \frac{3L\gamma_Q\gamma'(x_0)}{4\omega_0} - \frac{L[F_{\text{SF}}''(x_0) - p_0\gamma''(x_0)]}{2M\omega_0}, \tag{E10}$$

$$J_9 = -\frac{L}{\hbar}\{F_{\text{SF}}(x_0) - p_0\gamma(x_0) + \Delta x_{\text{th}}^2[F_{\text{SF}}''(x_0) - p_0\gamma''(x_0)]\}. \tag{E11}$$

It is worthwhile to note that matrix M is block diagonal and only couples correlation functions Δ_{nm} of the same order $n + m$. Hence, squeezing and other modifications of correlation functions must be generated through the inhomogeneity $\vec{J}(t)$.

The solution of Eq. (E4) for $\vec{V}(0) = 0$ is given by

$$\vec{V}(t) = \int_0^t dt'\, e^{M(t-t')} \cdot \vec{J}(t'). \tag{E12}$$

This is best evaluated by using the eigenvalues of M. This matrix is not Hermitian, but it is not singular. We can therefore express any vector in the form

$$\vec{J}(t') = \sum_{\alpha=1}^9 \vec{e}_\alpha \tilde{J}_\alpha(t'), \tag{E13}$$

where $\vec{e}_\alpha$ are the eigenvectors of M. Specifically, the relationship between the original components J_i and the expansion coefficients $\tilde{J}_\alpha$ is given by

$$\tilde{J}_1 = \frac{J_9(2\omega_0 - i\gamma_Q)}{2\sqrt{2}\omega_0} - \frac{iJ_8}{\sqrt{2}} \tag{E14}$$

$$= -\frac{L}{\sqrt{2}\hbar}\left(1 - i\frac{\gamma_Q}{2\omega_0}\right)\{F_{\text{SF}}(x_0) - p_0\gamma(x_0) + \Delta x_{\text{th}}^2[F_{\text{SF}}''(x_0) - p_0\gamma''(x_0)]\}, \tag{E15}$$

$$\tilde{J}_3 = \frac{J_2\gamma_Q}{\sqrt{2}\omega_0} + \frac{J_1}{\sqrt{2}} + \frac{J_3}{\sqrt{2}} \tag{E16}$$

$$= -\frac{\sqrt{2}M\omega_0\Delta x_{\text{th}}^4[\gamma'(x_0)^2 + \gamma(x_0)\gamma''(x_0)]}{\hbar\gamma(x_0)} - \frac{\gamma_Q\left(\Delta x_{\text{th}}^2 - \frac{L^4}{16\Delta x_{\text{th}}^2}\right)[F_{\text{SF}}'(x_0) - p_0\gamma'(x_0)]}{\sqrt{2}\hbar\omega_0} - \frac{\hbar[\gamma'(x_0)^2 - 3\gamma(x_0)\gamma'(x_0)]}{8\sqrt{2}M\omega_0\gamma(x_0)}, \tag{E17}$$

$$\tilde{J}_4 = \frac{\sqrt{3}J_3(\omega_0 - i\gamma_Q)}{4\omega_0} - \frac{\sqrt{3}J_2(\gamma_Q + 2i\omega_0)}{4\omega_0} - \frac{1}{4}\sqrt{3}J_1 \tag{E18}$$

$$= \frac{\sqrt{3}\hbar\{4M\omega_0^2\gamma(x_0) + (3\gamma_Q + 2i\omega_0)[F'_{\text{SF}}(x_0) - p_0\gamma'(x_0)]\}}{64M^2\omega_0^3\Delta x_{\text{th}}^2} + \frac{\sqrt{3}\Delta x_{\text{th}}^2(\gamma_Q + 2i\omega_0)[F'_{\text{SF}}(x_0) - p_0\gamma'(x_0)]}{4\omega_0\hbar}$$

$$+ \frac{i\sqrt{3}M\Delta x_{\text{th}}^4(\gamma_Q + i\omega_0)[\gamma'(x_0)^2 + \gamma(x_0)\gamma''(x_0)]}{2\hbar\gamma(x_0)} + \frac{i\sqrt{3}\hbar(\gamma_Q + i\omega_0)[\gamma'(x_0)^2 - 3\gamma(x_0)\gamma''(x_0)]}{32M\omega_0^2\gamma(x_0)}, \tag{E19}$$

$$\tilde{J}_6 = \frac{\sqrt{5}J_7(2\omega_0 - i\gamma_Q)}{8\omega_0} + \frac{\sqrt{5}J_5(2\omega_0 - 3i\gamma_Q)}{8\omega_0} + \frac{\sqrt{5}J_6(\gamma_Q - i\omega_0)}{4\omega_0} - \frac{1}{4}i\sqrt{5}J_4 \tag{E20}$$

$$= -\frac{\sqrt{5}(\gamma_Q - i\omega_0)}{L^3\omega_0}\Delta x_{\text{th}}^4\gamma'(x_0) + \frac{\sqrt{5}(\gamma_Q - i\omega_0)}{4\omega_0}L\Delta x_{\text{th}}^2\gamma^{(3)}(x_0)$$

$$+ \frac{\sqrt{5}L}{16M\omega_0^2}\{(i\gamma_Q - 2\omega_0)[F''_{\text{SF}}(x_0) - p_0\gamma''(x_0)] + 3(2\gamma_q - i\omega_0)M\omega_0\gamma'(x_0)\}, \tag{E21}$$

$$\tilde{J}_8 = \frac{J_7(2\omega_0 - 3i\gamma_Q)}{8\omega_0} - \frac{3J_6(\gamma_Q + i\omega_0)}{4\omega_0} + \frac{3iJ_5(\gamma_Q + 2i\omega_0)}{8\omega_0} + \frac{iJ_4}{4} \tag{E22}$$

$$= \frac{3\Delta x_{\text{th}}^4(\gamma_Q + i\omega_0)\gamma'(x_0)}{L^3\omega_0} - \frac{3L\Delta x_{\text{th}}^2\gamma^{(3)}(x_0)(\gamma_Q + i\omega_0)}{4\omega_0}$$

$$- \frac{L}{16M\omega_0^2}\{(2\omega_0 - 3i\gamma_Q)[F''_{\text{SF}}(x_0) - p_0\gamma''(x_0)] + 3M\omega_0(2\gamma_Q + 3i\omega_0)\gamma'(x_0)\}, \tag{E23}$$

and $\tilde{J}_2 = \tilde{J}_1^*$, $\tilde{J}_5 = \tilde{J}_4^*$, $\tilde{J}_7 = \tilde{J}_6^*$, and $\tilde{J}_9 = \tilde{J}_8^*$. For $\gamma_Q \ll \omega_0$, the eigenvalues of M are approximately given by

$$\lambda_\alpha \in \left\{ -\frac{\gamma_Q}{2} - i\omega_0, -\frac{\gamma_Q}{2} + i\omega_0, -\gamma_Q, -\gamma_Q - 2i\omega_0, -\gamma_Q + 2i\omega_0, -\frac{3\gamma_Q}{2} - i\omega_0, -\frac{3\gamma_Q}{2} + i\omega_0, -\frac{3\gamma_Q}{2} - 3i\omega_0, -\frac{3\gamma_Q}{2} + 3i\omega_0 \right\}, \tag{E24}$$

which leads to

$$\vec{V}(t) = \sum_{\alpha=1}^{9} \vec{e}_\alpha \int_0^t dt'\, e^{\lambda_\alpha(t-t')}\tilde{J}_\alpha(t'). \tag{E25}$$

From this expression, we can draw several conclusions. (i) First-order perturbative effects on *mean position and momentum* are described through terms involving $\tilde{J}_1$ and $\tilde{J}_2$ in solution (E25). These terms are not affected by quantum effects. They are affected by thermal fluctuations through terms proportional to Δx_{th} in Eq. (E15), but a numerical estimate shows that this influence is small, roughly on the order of 10^{-4}. Therefore, in agreement with numerical simulations, we conclude that the point-particle approximation is appropriate if only the position of the tip is measured. (ii) Terms involving

$\tilde{J}_6$ to $\tilde{J}_9$ describe the influence of the surface force and quantum effects on *skewness*. Numerical simulations show that the overall size of skewness remains small, so that we do not discuss the details of this case. (iii) The third-order expansion presented above is sufficient to describe squeezing and skewness for up to 300 cycles of the cantilever. For longer times, fourth-order terms (coupling to variances Δ_{nm} with $n + m = 4$) can have a strong influence on squeezing and skewness. We have analyzed the corresponding coupling numerically, but since it is not relevant for normal AFM time scales we do not discuss it here. (iv) *Squeezing* of second-order variances is the most interesting case, since it may be observable and exhibits the largest contributions due to quantum dynamics. Squeezing is introduced through terms involving $\tilde{J}_3$ to $\tilde{J}_5$. To first order in γ_Q, the corresponding eigenvectors of M are given by

$$\vec{e}_3 = \left(\frac{1}{\sqrt{2}}, -\frac{\gamma_Q}{2\sqrt{2}\omega 0}, \frac{1}{\sqrt{2}}, 0, 0, 0, 0, 0, 0 \right), \tag{E26}$$

$$\vec{e}_4 = \left(-\frac{1}{\sqrt{3}} - \frac{i\gamma_Q}{\sqrt{3}\omega_0}, -\frac{\gamma_Q}{2\sqrt{3}\omega_0} + \frac{i}{\sqrt{3}}, \frac{1}{\sqrt{3}}, 0, 0, 0, 0, 0, 0 \right), \tag{E27}$$

and $\vec{e}_5 = \vec{e}_4^*$. In this expression, the first three components correspond to position variance, Δ_{11}, and momentum variance, respectively. For brevity, we will only discuss the position variance, for which Eq. (E25) yields

$$\Delta_{20}^{(1)} = \int_0^t dt'\, e^{\gamma_Q(t'-t)}\left[\frac{\gamma_Q\left(\frac{L^4}{16} - \Delta x_{\text{th}}^4\right)}{2M\omega_0^2\Delta x_{\text{th}}^2}[F'_{\text{SF}}(x_0(t')) - p_0(t')\gamma'(x_0(t'))] - \left(\Delta x_{\text{th}}^4 - \frac{3L^4}{16}\right)\gamma''(x_0(t')) - \left(\frac{L^4}{16} + \Delta x_{\text{th}}^4\right)\frac{\gamma'(x_0(t'))^2}{\gamma(x_0(t'))} \right]$$

$$+ \int_0^t dt'\, \frac{e^{\gamma_Q(t'-t)}\cos[2\omega_0(t-t')]}{\Delta x_{\text{th}}^2}\left[\Delta x_{\text{th}}^2\left(\Delta x_{\text{th}}^4 - \frac{3L^4}{16}\right)\gamma''(x_0(t')) - \frac{L^4}{8}\gamma(x_0(t')) \right.$$

$$- \frac{\gamma_Q}{2M\omega_0^2}\left(\frac{L^4}{16} - \Delta x_{\text{th}}^4\right)[F'_{\text{SF}}(x_0(t')) - p_0(t')\gamma'(x_0(t'))] + \Delta x_{\text{th}}^2\left(\frac{L^4}{16} + \Delta x_{\text{th}}^4\right)\frac{\gamma'(x_0(t'))^2}{\gamma(x_0(t'))}\Bigg]$$

$$- \int_0^t dt' \frac{e^{\gamma_Q(t'-t)}\sin[2\omega_0(t-t')]}{M\omega_0\Delta x_{\text{th}}^2}\left[\left(\frac{L^4}{16} + \Delta x_{\text{th}}^4\right)[F'_{\text{SF}}(x_0(t')) - p_0(t')\gamma'(x_0(t'))] + \frac{L^4}{8}M\gamma_Q\gamma(x_0(t'))\right]. \tag{E28}$$

This expression shows that quantum effects are generally very small. They enter through the ground-state width L, which, at room temperature, is about a factor of 10^{-4} smaller than the thermal variance Δx_{th} of the tip position.

To gain a better understanding of quantum effects, we have analyzed this expression for the special case of a single-frequency driving force [$F_2 = 0$ in Eq. (2)] oscillating at resonance frequency, $\omega_1 = \omega_0$. Furthermore, we concentrate on the effect of a dissipative surface force of the form (B12). The integral then reduces to Eq. (14). The implications of this result are discussed in the main text.

APPENDIX F: COMMUTATORS OF FUNCTIONS OF POSITION AND MOMENTUM

We consider functions of operator $\hat{x}$ and want to evaluate commutators of the form

$$X_n = [V(\hat{x}), \hat{p}^n]. \tag{F1}$$

We note that, since the commutator between $\delta\hat{x}$ and $\delta\hat{p}$ of Eqs. (B6) and (B7) is the same as that of $\hat{x}$ and $\hat{p}$, our results are also valid for commutators of the form $[V(\delta\hat{x}), \delta\hat{p}^n]$.

Lemma 1.

$$X_n = i\sum_{l=1}^n c_{n,l}\hbar^l R^{(n-l)}(V^{(l)}), \tag{F2}$$

$$R^{(m)}(f(\hat{x})) = \hat{p}^m f(\hat{x}) + f(\hat{x})\hat{p}^m, \tag{F3}$$

with coefficients $c_{n,l}$ that need to be determined.

Proof. For $n = 1$ we have

$$X_1 = i\hbar c_{1,1} R^{(0)}(V^{(1)}), \tag{F4}$$

with $c_{1,1} = \frac{1}{2}$. Assuming relation (F2) holds for $n-1$, we obtain

$$X_n = i\left(\frac{\hbar}{2}R^{(n-1)}(V') + \frac{1}{2}\sum_{r=1}^{n-1} c_{n-1,r}\hbar^r\left[\hat{p}R^{(n-1-r)}(V^{(r)}) + R^{(n-1-r)}(V^{(r)})\hat{p}\right]\right). \tag{F5}$$

Now,

$$\hat{p}R^{(m)}(f) + R^{(m)}(f)\hat{p} = 2R^{(m+1)}(f) + \sum_{k=1}^m c_{m,k}\hbar^{k+1}R^{(m-k)}(f^{(k+1)}), \tag{F6}$$

so that

$$X_n = i\left(\frac{\hbar}{2}R^{(n-1)}(V') + \sum_{l=1}^{n-1} c_{n-1,l}\hbar^l R^{(n-l)}(V^{(l)}) + \frac{1}{2}\sum_{r=1}^{n-2} c_{n-1,r}\sum_{k=1}^{n-1-r} c_{n-1-r,k}\hbar^{r+k+1}R^{(n-1-r-k)}(V^{(r+k+1)})\right). \tag{F7}$$

Introducing the new summation index $l = r + k + 1$, we find

$$X_n = i\left(\frac{\hbar}{2}R^{(n-1)}(V') + \sum_{l=1}^{n-1} c_{n-1,l}\hbar^l R^{(n-l)}(V^{(l)}) + \frac{1}{2}\sum_{l=3}^n \hbar^l R^{(n-l)}(V^{(l)})\sum_{r=1}^{l-2} c_{n-1,r}c_{n-1-r,l-r-1}\right) \tag{F8}$$

$$= i\sum_{l=1}^n c_{n,l}\hbar^l R^{(n-l)}(V^{(l)}), \tag{F9}$$

with

$$c_{n,1} = \tfrac{1}{2} + c_{n-1,1}, \tag{F10}$$

$$c_{n,2} = c_{n-1,2}, \tag{F11}$$

$$c_{n,l} = c_{n-1,l} + \frac{1}{2}\sum_{r=1}^{l-2} c_{n-1,r}c_{n-1-r,l-r-1} \quad \text{for } 3 \leqslant l \leqslant n. \tag{F12}$$

This completes the proof of Lemma 1.

Equation (F12) provides us with a recursion relation that can be used to determine all factors $c_{n,l}$. We have verified that, up to $n = 15$, these factors correspond to coefficients of Euler polynomials $E_n(x)$. More specifically, we found that

$$\sum_{l=1}^{n} c_{n,l} x^{n-l} = i(i^n E_n(-ix) - x^n). \tag{F13}$$

We can now introduce superoperators defined by

$$\overrightarrow{\mathcal{P}}^m V(\hat{x}) = \left(\frac{\hat{p}^m}{\hbar \frac{\partial}{\partial \hat{x}}}\right)^m V(\hat{x}), \tag{F14}$$

$$\overleftarrow{\mathcal{P}}^m V(\hat{x}) = \left(\frac{1}{\hbar \frac{\partial}{\partial \hat{x}}}\right)^m V(\hat{x}) \hat{p}^m, \tag{F15}$$

to write the commutation relations in a compact form:

$$[V(\hat{x}), \hat{p}^n] = -\left(\hbar \frac{\partial}{\partial \hat{x}}\right)^n [i^n E_n(-i\overrightarrow{\mathcal{P}}) - \overrightarrow{\mathcal{P}}^n$$
$$+ i^n E_n(-i\overleftarrow{\mathcal{P}}) - \overleftarrow{\mathcal{P}}^n]V(\hat{x}). \tag{F16}$$

It may appear strange that a derivative operator appears in the denominator of superoperators $\overleftrightarrow{\mathcal{P}}$. However, no negative powers of derivative operators appear in result (F16). We remark that a similar result for quadratic potentials has been proven by De Angelis and Vignat [54].

An important special case is when the function is a power, $V(\hat{x}) = \hat{x}^m$. It is easy to see that the (mean value of the) commutator then reduces to

$$\langle[\delta\hat{x}^m, \delta\hat{p}^n]\rangle = 2i \sum_{l=1}^{\min(m,n)} \binom{m}{l} \frac{c_{n,l}\hbar^l}{l!} \Delta_{m-l,n-l}. \tag{F17}$$

---

[1] H. Lüth, *Solid Surfaces, Interfaces and Thin Films* (Springer, New York, 2015).

[2] G. Binnig, C. F. Quate, and C. Gerber, Phys. Rev. Lett. **56**, 930 (1986).

[3] N. Gavara, Microsc. Res. Tech. **80**, 75 (2017).

[4] S. N. Magonov and M. Whangbo, *Surface Analysis with STM and AFM: Experimental and Theoretical Aspects of Image Analysis* (Wiley, New York, 2008).

[5] P. Hinterdorfer and Y. Dufrêne, Nat. Methods **3**, 347 (2006).

[6] A. Quigley, S. P. Veres, and L. Kreplak, PLoS One **11**, e0161951 (2016).

[7] G. Pyrgiotakis, C. O. Blattmann, and P. Demokritou, ACS Sustainable Chem. Eng. **2**, 1681 (2014).

[8] R. García and R. Pérez, Surf. Sci. Rep. **47**, 197 (2002).

[9] D. Platz, E. Tholén, D. Pesen, and D. Haviland, Appl. Phys. Lett. **92**, 153106 (2008).

[10] J. R. Lozano and R. Garcia, Phys. Rev. Lett. **100**, 076102 (2008).

[11] R. Garcia and E. Herruzo, Nat. Nanotechnol. **7**, 217 (2012).

[12] Y. F. Dufrêne, T. Ando, R. Garcia, D. Alsteens, D. Martinez-Martin, A. Engel, C. Gerber, and D. J. Müller, Nat. Nanotechnol. **12**, 295 (2017).

[13] C. Amo, A. Perrino, A. Payam, and R. Garcia, ACS Nano **11**, 8650 (2017).

[14] V. Gisbert, C. Amo, M. Jaafar, A. Asenjo, and R. Garcia, Nanoscale **13**, 2026 (2021).

[15] M. Kisiel, F. Pellegrini, G. E. Santoro, M. Samadashvili, R. Pawlak, A. Benassi, U. Gysin, R. Buzio, A. Gerbi, E. Meyer, and E. Tosatti, Phys. Rev. Lett. **115**, 046101 (2015).

[16] E. Gnecco, R. Pawlak, M. Kisiel, T. Glatzel, and E. Meyer, *Nanotribology and Nanomechanics* (Springer, New York, 2017), pp. 519–548.

[17] A. Passian and G. Siopsis, Phys. Rev. A **94**, 023812 (2016).

[18] A. Passian and G. Siopsis, Phys. Rev. A **95**, 043812 (2017).

[19] D. Rugar and P. Grütter, Phys. Rev. Lett. **67**, 699 (1991).

[20] L. Mandel and E. Wolf, *Optical Coherence and Quantum Optics* (Cambridge University, New York, 1995).

[21] C. W. Gardiner and P. Zoller, *Quantum noise* (Springer-Verlag, Berlin, 2004).

[22] A. Caldeira and A. Leggett, Ann. Phys. (NY) **149**, 374 (1983).

[23] *Cavity Optomechanics: Nano- and Micromechanical Resonators Interacting with Light*, edited by M. Aspelmeyer, T. Kippenberg, and F. Marquardt (Springer, New York, 2014).

[24] W. Bowen and G. Milburn, *Quantum Optomechanics* (CRC, Boca Raton, FL, 2016).

[25] R. Riedinger, A. Wallucks, I. Marinković, C. Löschnauer, M. Aspelmeyer, S. Hong, and S. Gröblacher, Nature (London) **556**, 473 (2018).

[26] L. Mercier de Lépinay, C. F. Ockeloen-Korppi, M. J. Woolley, and M. A. Sillanpää, Science **372**, 625 (2021).

[27] H. Yu *et al.*, Nature (London) **583**, 43 (2020).

[28] E. L. Hahn, Phys. Rev. **80**, 580 (1950).

[29] T. W. Hänsch, S. A. Lee, R. Wallenstein, and C. Wieman, Phys. Rev. Lett. **34**, 307 (1975).

[30] K.-P. Marzlin and J. Audretsch, Phys. Rev. A **53**, 312 (1996).

[31] B. Dubetsky and M. A. Kasevich, Phys. Rev. A **74**, 023615 (2006).

[32] J. S. Pedernales, G. W. Morley, and M. B. Plenio, Phys. Rev. Lett. **125**, 023602 (2020).

[33] B. Pottier and L. Bellon, Appl. Phys. Lett. **110**, 094105 (2017).

[34] S. Benaglia, C. Amo, and R. Garcia, Nanoscale **11**, 15289 (2019).

[35] K. Johnson, K. Kendall, A. Roberts, and D. Tabor, Proc. R. Soc. A **324**, 301 (1971).

[36] H. Dankowicz and M. R. Paul, Eng. Syst. Des. Anal. **2**, 633 (2008).

[37] E. H. Lee and J. R. M. Radok, J. Appl. Mech. **27**, 438 (1960).

[38] T. C. T. Ting, J. Appl. Mech. **33**, 845 (1966).

[39] D. Platz, D. Forchheimer, E. A. Tholén, and D. B. Haviland, Nat. Commun. **4**, 1360 (2013).

[40] A. Spanos, *Probability Theory and Statistical Inference: Econometric Modeling with Observational Data* (Cambridge University, New York, 1999).

[41] J. Liouville, J. Math. Pures Appl. **3**, 342 (1838).

[42] R. F. Streater and A. S. Wightman, *PCT, Spin and Statistics and All That* (Princeton University, Princeton, NJ, 1964).

[43] A. Azzalini and A. D. Valle, Biometrika **83**, 715 (1996).

[44] A. Ahlin, Noise squeezing and parametric amplification in dynamic AFM, Master's thesis, Royal Institute of Technology (KTH), 2018.

[45] E. Herruzo and R. Garcia, Beilstein J. Nanotechnol. **3**, 198 (2012).

[46] H. Callen and T. Welton, Phys. Rev. **83**, 34 (1951).

[47] R. Kubo, Rep. Prog. Phys. **29**, 255 (1966).

[48] C. Cercignani, V. Gerasimenko, and D. Petrina, *Many-Particle Dynamics and Kinetic Equations* (Springer, New York, 1997).

[49] A. D. Fokker, Ann. Phys. (Leipzig) **348**, 810 (1914).

[50] M. Planck, Sitzungsber. Preuss. Akad. Wiss. Berlin Phys. Math. Kl. **24**, 324 (1917).

[51] G. Lindblad, Commun. Math. Phys. **48**, 119 (1976).

[52] K. Hornberger, Lect. Notes Phys. **768**, 221 (2009).

[53] D. P. E. Smith, Rev. Sci. Instr. **66**, 3191 (1995).

[54] V. De Angelis and C. Vignat, J. Math. Phys. **56**, 123506 (2015).

[55] In all our calculations, we have expressed x in units of the harmonic oscillator ground state width $L = \sqrt{\hbar/(M\omega_0)}$ and momentum in units of $\hbar/L$.

[56] The momentum units used in the graphs may appear unusual. Squeezing is best observed if position and momentum are measured in units of L and $\hbar/L$, respectively. In this case, position and momentum uncertainties are equal, both for the quantized ground state of the oscillator and for a thermal classical distribution. We have used these natural squeezing units in our calculations. For the graphs, we have used the same rescaling factor for position and momentum to represent position in picometers. As a consequence, momentum is then measured in $\hbar$ over attometers.